nature chemical biology

Article

https://doi.org/10.1038/s41589-025-02085-x

# Ideal efficacy photoswitching for chromocontrol of TRPC4/5 channel functions in live tissues

Received: 29 December 2024

Accepted: 31 October 2025

Published online: 16 January 2026

Check for updates

Markus Müller[1,2,9], Konstantin Niemeyer[3,9], Navin K. Ojha[4], Sebastian A. Porav[5,6], Deivanayagabarathy Vinayagam[7], Nicole Urban[3], Fanny Büchau[3], Katharina Oleinikov[4], Mazen Makke[4], Claudia C. Bauer[5,6], Aidan V. Johnson[5,6], Stephen P. Muench[6,8], Frank Zufall[4], Dieter Bruns[4], Yvonne Schwarz[4], Stefan Raunser[7], Trese Leinders-Zufall[4], Robin S. Bon[5,6], Michael Schaefer[3,10] ✉ & Oliver Thorn-Seshold[1,10] ✉

Precisely probing the endogenous roles of target proteins is crucial for biological research. Photochemical tools can be photoactuated with high spatiotemporal resolution but often they are unreliable in vivo because spatiotemporal variations of reagent concentration result in inhomogeneous bioactivity. We now describe ideal efficacy photoswitching, a paradigm that internally compensates for reagent concentration by self-competitive binding, allowing purely wavelength-dependent chromocontrol over bioactivity that is consistent from cell culture to deep tissues. We demonstrate this with photoswitches for endogenous transient receptor potential (TRP) C4 and C5 ion channels, reproducibly delivering strong agonism under 360-nm illumination, weak agonism under 385-nm illumination and strong antagonism under 440-nm illumination. These ligands unlock a range of high-precision investigations in TRP biology, from neuronal activity to exocytosis, reproductive signaling and smooth muscle contractility. The ideal efficacy photoswitching paradigm should also unlock high-performance chromocontrol over a wide range of sensory or signaling channels and receptors even in vivo.

The 27 human transient receptor potential (TRP) proteins can assemble to form tetrameric TRP cation channels, which have varied and highly tissue-dependent roles in cellular physiology, from sensing and signaling to mineralostasis[1,2]. Several environment-sensing TRP channels such as TRPV1 (heat), TRPM8 (cold) or TRPA1 (electrophiles) are well studied. The roles and importance of many other TRP channels remain unclear, even though their links with diseases make them hotly pursued as therapeutic targets[3–5]. The structurally similar TRPC4 and TRPC5 (TRPC4/5) are mainly expressed in the central nervous system, gut and kidneys[6–8], where they are linked with pain[9–11], reproductive signaling[12], anxiety and depression[13,14], kidney disease[15] and digestion[16]; striking discoveries are still ongoing, for example, linking TRPC5 loss to postpartum depression and obesity[17]. TRPC4/5 form both homotetrameric and heterotetrameric functional channels that can also include TRPC1 (ref. 18).

Insights into TRPC4/5 relevance were initially derived from knockout mice because potent and selective modulators were lacking[19]. Recently, small-molecule modulators of TRPC4/5 became available as tool compounds[20]: from the nanomolar-potent natural product (−)-englerin A (EA)[21], a TRPC1/4/5 activator[22,23], to drug candidate inhibitors (for example, TRPC4/5-targeting xanthines BI-1358894, HC-070 and Pico145/HC-608 developed by Hydra/Boehringer or TRPC5-targeting pyridazinones GFB-8438 and GFB-887 developed by GoldfinchBio) (Fig. 1a and Supplementary Note 1)[24,25]. However, TRP

A full list of affiliations appears at the end of the paper. ✉e-mail: michael.schaefer@medizin.uni-leipzig.de; oliver.thorn-seshold@tu-dresden.de

functionality varies according to tissue localization (spatial) and TRPs are best studied if their activity is reversibly modulated on short timescales (temporal). Therefore, photoresponsive chemical tools, whose activity can be spatiotemporally patterned by light, are particularly promising to resolve TRP biology[26]. Photoswitchable TRP ligands have been impactful, with azo-capsaicins for TRPV1 (refs. 27,28), TRPswitch for TRPA1 (ref. 29), OptoBI for TRPC3 (ref. 30) and azo-diacylglycerols (PhoDAGs and OptoDArGs) for TRPC2/3/6 (refs. 31–33). However, there is no photoresponsive ligand for TRPC4 and the sole compound for Trpc5 (BTDAzo, a lipophilic photoswitchable agonist) has low potency and is almost inactive on human TRPC5 (ref. 34).

Here we sought to create potent, selective, photoswitchable TRPC4/5 modulators for spatiotemporally resolved TRP studies in complex systems. Xanthines such as HC-070 and Pico145 were our choice for parent ligands, as small chemical changes switch them from activators to inhibitors[35,36], in turn suggesting that a compound could be designed such that photoswitching it would likewise change its efficacy. We now report the design and experimental validation of this concept and use these tools for light-controlled high-precision elucidation of the separate roles of TRPC4 and TRPC5 from cell culture through to endogenous organ sections; as this efficacy switch paradigm solves systematic problems that have hampered the field of photopharmacology for decades, we argue for adopting it more broadly as a method to unlock high-precision in vivo chromocontrol of a range of biological systems.

## Results

### Design concept for efficacy switching

Azobenzenes are the best-explored chemical scaffolds for fully reversible structural photoswitching (through $E \leftrightarrows Z$ isomerization)[37] and we decided to use them in ligands to photoswitch TRPC4/5 bioactivity. However, azobenzene $E \leftrightarrows Z$ photoswitching is never complete in both directions: it operates between mostly *Z* and mostly *E* photostationary states (PSSs, typically ~90% *Z* for the mostly *Z*-PSS [*Z**] and ~80% *E* for the mostly *E*-PSS [*E**]).

Affinity switching is the typical pharmacological approach used for structure–activity relationship-based photopharmacology; for example, differences in the steric fit of *E* and *Z* isomers drive a difference in their binding affinity, such that net $E \leftrightarrows Z$ photoswitching modulates the target's biological activity. One well-known problem, even for a hypothetical 'ideal' affinity switch (with a completely nonbinding *E* isomer but a high-agonist-potency *Z* isomer; Fig. 1e), is the high background activity after typical $Z \rightarrow E$ photoswitching 'off' because of the typically 20% residual *Z* isomer in the mostly *E*-PSS. The generalized result is that bidirectional photocontrol of an affinity switch can only deliver a narrow functional dynamic range of bioactivity (FDR)[38,39], that is, the bioactivity window between the best photoswitched on and best photoswitched off states (Fig. 1f; the FDR is limited by its PSSs in both directions). In theory, this could be remedied by making affinity switches with bidirectionally complete photoswitching. Yet, there is a second systematic problem, which has long been ignored and cannot be fixed no matter how complete the photoswitching or, if fast $Z \rightarrow E$ relaxation is used, how extreme the affinity difference or how red-shifted the wavelengths. This problem is that the bioactivity applied under any given wavelength remains extremely sensitive to concentration (Fig. 1j), such that both dose and wavelength must be dynamically balanced to deliver a given effect. We suggest that this explains why the applicability of freely diffusing affinity switches for bidirectional photocontrol has been and will remain limited to highly controlled cell culture settings[40] where their concentration is effectively clamped (Supplementary Note 2). This is because, in tissue or in vivo, spatially variable reagent concentrations that also evolve heterogeneously over time (absorption, distribution, metabolism and excretion, pharmacokinetics, distance from blood vessels and interanimal variability) will prevent delivering a reliable, homogeneous effect.

Efficacy switching is the pharmacological[41] approach we use here, although we will have to newly define an 'ideal' class of efficacy photoswitch, with importantly distinct properties, to reach its potential. An efficacy photoswitch is a reagent whose *E*/*Z* photoisomers exert different efficacies on a target. Unhelpfully, this covers reagents of limited practical utility, for example, whose *E*/*Z* isomers have similar degrees of the same efficacy (for example, 60% versus 70% partial agonism), such that biologically applicable photocontrol is impossible, or whose *E*/*Z* isomers have very different affinity (typically ≥10×), such that, in practice, they act as affinity switches with their associated problems and/or whose *E*/*Z* isomers have such low affinity (for example, half-maximal effective concentration ($EC_{50}$) > 1 µM) that the reagent cannot be reliably applied at saturation (>10 × $EC_{50}$) and, thus, cannot overcome concentration inhomogeneities. Any one of these problems makes an efficacy photoswitch nonideal.

We, therefore, define an ideal efficacy photoswitch as a reagent whose *E*/*Z* isomers bind competitively to each other, with identical or very similar affinity, whose *E*/*Z* isomers have opposing activity, for example, activator/inhibitor (or else one isomer is a silent binder) (Fig. 1h), and where both *E*/*Z* isomers have high potency such that plateau concentrations of 10–100 × $EC_{50}$ can be reliable applied (for example, both $EC_{50}$ < 50 nM). The novelty of creating such a nanomolar ideal efficacy switch on TRPC4/5-binding scaffolds is the chemical highlight of this paper and is the key to their biological utility. First however, it will be crucial to trace two advantages of ideal efficacy switching, as the pharmacological issue of how a compound exerts its photocontrol has not yet received proper formal attention (especially compared to, for example, how much literature is devoted to easily measured but less critical aspects such as incremental tuning of photoresponse wavelengths and PSSs).

(1) Chromocontrol is biologically practical: For an ideal efficacy switch, above a threshold for the total *E*/*Z* concentration where its target nears saturation by any *E*/*Z* mixture (~5 × $EC_{50}$), there is no more concentration dependency of bioactivity. The only variable controlling bioactivity is the *E*/*Z* ratio of the competitively binding isomers: that is, the applied color (wavelength) of light sets the PSS, which entirely controls the bioactivity on the target. Just shifting the wavelength can rheostat the target to, for example, strongly on, weakly on, baseline or strongly inhibited states. We now specifically term this target 'chromocontrol', from the Greek *chromos* (color); this distinguishes it from 'photocontrol' that is used to indicate a general response to light often with affinity switches, but never with the implication of concentration-independent chromocontrol (Fig. 1g,i). Reproducibly and homogeneously applying a specific wavelength of light is far easier than trying to achieve reproducible, homogeneous drug concentrations even across in vitro models, let alone in vivo, suiting efficacy switches to easy translation between model systems and making them ideal or even irreplaceable to tackle complex environments.

(2) Chromocontrol is biologically meaningful: Only plateau regions in dose–response curves can be used robustly when concentrations are variable. As an efficacy photoswitch's bioactivity is equally controlled by wavelength at any concentration above its threshold, the working concentration window within which a biological effect is (identically) PSS dependent is vast (Fig. 1g,i). Furthermore, even a hypothetical ideal affinity switch only has two plateau effect values (full on/full off; Fig. 1f); hence, when concentrations are variable, the switch can only reliably be applied for full on and full off photocontrol. By contrast, ideal efficacy switches, with wavelength-dependent plateaus across their full effect range (for example, strongly on, weakly on, baseline and strongly inhibited), allow reliable rheostatting of bioactivity, which can be more nuanced and biologically meaningful (for example Fig. 6g,h).

https://doi.org/10.1038/s41589-025-02085-x

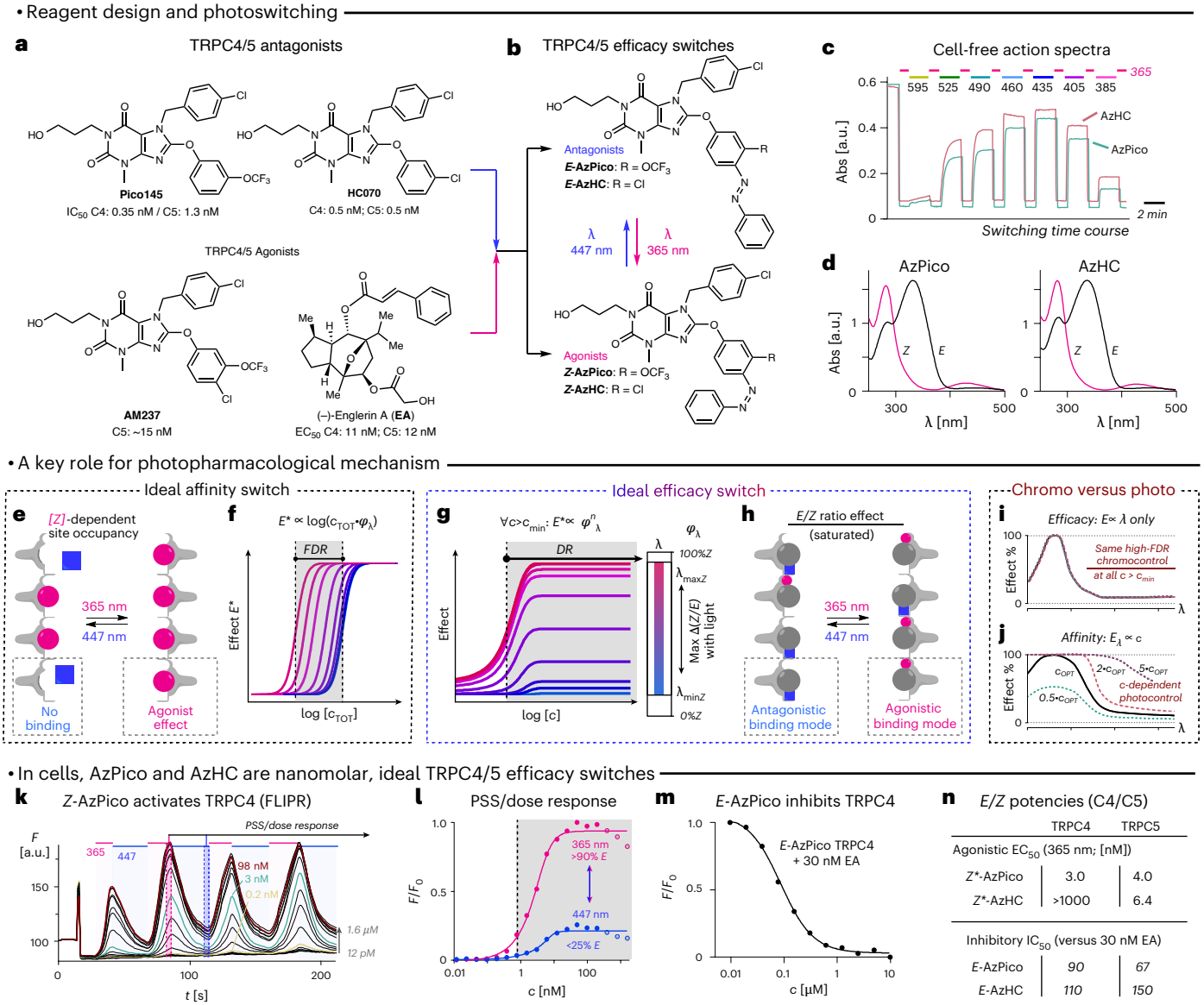


**Fig. 1 | Ideal efficacy photoswitches for TRPC4/5. a**, Known TRPC4/5 modulators. **b**, Photoswitchable TRPC4/5 modulators AzPico and AzHC. **c**,**d**, Photoisomerization action spectra and *E*/*Z* isomer absorption spectra (derived for individual isomers from high-performance liquid chromatography) of AzPico and AzHC. **e**,**f**, For an ideal affinity switch, only one isomer binds the target. Within the FDR window, the binding site occupancy and, thus, biological effect $E^*$ depend on the total switch concentration $c_{TOT}$ and the PSS fraction of active isomer $\varphi_\lambda$. **g**,**h**, For an ideal efficacy switch, both isomers bind with similar affinities but with different efficacies. The dynamic range (DR) where the biological effect $E^*_\lambda$ is PSS dependent but concentration independent covers all $c > c_{min}$. **i**,**j**, Chromocontrol in practice: for an efficacy switch, small variations in PSS(λ) sensitively control performance (whereas, in affinity switches, they are unimportant) but even large variations in concentration, which would ruin the performance of an affinity switch, are irrelevant. **k**,**l**, Reversible $Ca^{2+}$ influx modulation with AzPico under 365/447-nm cycles, as time courses and peak amplitudes. **m**, *E*-AzPico binds competitively to EA. **n**, $EC_{50}$ and half-maximal inhibitory concentration values of *E*/*Z*-AzPico and AzHC on TRPC4 and TRPC5. **k**–**n**, Fluo-4-loaded $HEK_{mTRPC4\beta}$ cells.

These features should make efficacy photoswitches much better suited for robust and sensitive use in biology, from cell culture through to in vivo (Figs. 3–6). However, only a dozen cases of efficacy photoswitching have been published openly (chemokine, adenosine, cannabinoid, adrenergic and serotonin receptors). Key contributions include those of Leurs, Decker, Gorostiza and coworkers (details in Supplementary Note 2)[42–53]. However, these all class as nonideal, typically because (1) the ligand efficacies were switched between more and less activating, rather than, for example, activating and inhibiting and (2) the isomers' affinity was very different, which compromised the concentration independence of ideal efficacy switching. The closest to ideality was the Leurs chemokine photoswitch VUF16216 (refs. 43,48); however, it had micromolar activity that prevented it from exploiting effect plateaus for chromocontrol. Several other efficacy switches have been created but were not understood as such. For example, we published one reagent[34] whose excellent bioactivity photocontrol despite $E \leftrightarrows Z$ photoswitching incompleteness (a hallmark of efficacy switching) we failed to understand. Moreover, we believe that many more instances of unsuspected efficacy switches may be found by reparsing the literature (Supplementary Note 2 has examples from Fuchter, Groschner, Pepperberg, Trauner, etc.[29,30,54–56]).

We give this level of detail as we believe that ideal efficacy photoswitching is both necessary and sufficient to reach the naively popular picture of 'light control over biology', which motivated much of the photopharmacology over the last decades. We also did not find it collected accessibly in the literature elsewhere. However, the conceptual

https://doi.org/10.1038/s41589-025-02085-x

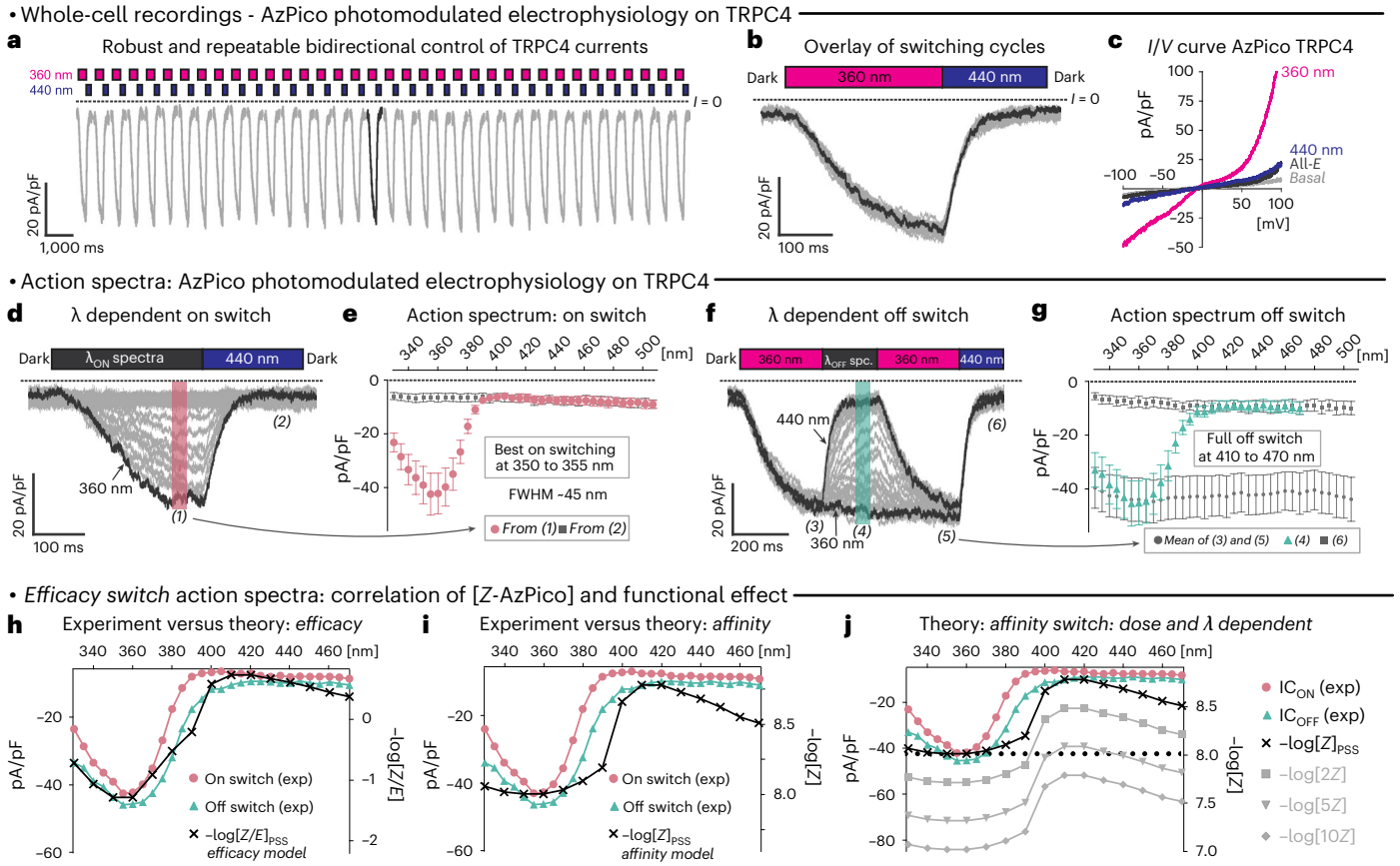


**Fig. 2 | AzPico-chromocontrolled electrophysiology of TRPC4.** **a**–**g**, Electrophysiological whole-cell recordings of TRPC4 currents in voltage clamp mode (**a**,**b**,**d**–**g**, $V_h$ = −80 mV; **c**, $V_h$ scan) in HEK293 cells with 10 nM AzPico during photoswitching. **a**,**b**, Reproducibility of 36 consecutive photoswitching cycles of 360/440 nm (**a**, time course; **b**, overlay of all cycles). **c**, *I*/*V* curves showing that 440 nm drives almost a full return to baseline currents throughout the applied voltage range. **d**–**g**, Spectral scans to extract the wavelength dependency of channel current photoswitching on (**d**,**e**, cycles of $\lambda_{ON}$/440 nm) and photoswitching off (**f**,**g**, 360 nm/$\lambda_{OFF}$). In **e**,**g**, $n$ = 12 biological replicates; data are presented as the mean values ± s.e.m. **h**–**j**, Electrophysiology action spectra of AzPico match PSS-based expectations for an efficacy switch (**h**) but not an affinity switch (**i**), which is an important distinction, as an affinity switch would have severely concentration-dependent activity (**j**) (full legend in Supplementary Information).

importance of this framework goes deeper than pharmacology. As one example, we highlight that there are target-driven reasons to choose efficacy switching for proteins that are natively poised for steeply nonlinear dose–response switching between metastable states, such as receptors and ion channels with multiple binding sites. These ought to be ideal platforms where the competitive binding of similar-affinity *E*/*Z* isomers with opposing modes of action ought to allow concentration-independent, rheostatted chromocontrol over protein activity, even when *E*⇆*Z* photoswitching is incomplete (see Discussion). A separate theoretical paper will treat these aspects in detail; however, for now, we set out to test this concept in practice, by creating such 'ideal efficacy switch' reagents for TRPC4/5.

## Creating xanthine efficacy switches

Xanthines Pico145 (also called HC-608) and HC-070 (ref. 57) are TRPC1/4/5 antagonists with picomolar potency[58] and remarkable selectivity against hundreds of enzymes, receptors, transporters and other ion channels (including other TRP channels)[24]. Excitingly, the very similar AM237 (ref. 57) is instead a nanomolar agonist of homotetrameric TRPC5, despite also being a nanomolar antagonist of homotetrameric TRPC4 (full details of pharmacology in Supplementary Note 1)[35]. The structures of these compounds with different efficacy are nearly identical (Pico145: *m*-$OCF_3$, HC-070: *m*-Cl; AM237: *m*-$OCF_3$, *p*-Cl; Fig. 1a). This suggests that the *meta*/*para* positions are suitable as an 'ideal efficacy tipping point', whereby small modifications may flip the efficacy mode (activator or inhibitor) without changing the binding affinity. Overall, the xanthines seem to be an outstanding starting point for ideal efficacy switches that are also highly potent; thus, they can be reliably applied in vivo.

In brief, we synthesized a series of xanthines 'extended' with bidirectionally switchable azobenzenes (Supplementary Fig. 3). Noteworthily, with a simple NNPh motif in *para* (where AM237 has a -Cl), we obtained AzPico (*m*-$OCF_3$) and AzHC (*m*-Cl; Fig. 1b), which were soon identified as the most biologically useful candidates in our panel of eight. From here onward, we focus only on them, leaving the others to Supplementary Note 3. AzPico/AzHC could be reversibly photoswitched between PSSs of ~82%*E* around 410 nm and 95%*Z* around 360 nm (Fig. 1c,d, and Supplementary Table 3).

## Parallel-throughput chromocontrol assessment in cells by FLIPR

We initially screened for the photoswitchability of activity in cells using a fluorometric imaging plate reader (FLIPR) calcium flux assay, with HEK293 cells stably expressing mouse TRPC4β or mouse TRPC5. Note, however, that the parallel-throughput FLIPR setup is limited to use fixed light-emitting diodes at 365 nm (good *Z*) and 447 nm (suboptimal *E*), which, combined with the slowness of the onset and recovery of the fluorescence readout for calcium, causes the FLIPR results to underestimate the reagents' true speed, degree and completion of TRPC chromocontrol (shown later).

*E*-AzPico from 12 pM to 1.6 µM gave no effect with TRPC4 or TRPC5; upon 365-nm illumination, strong agonism was evident with $Ca^{2+}$ influx

https://doi.org/10.1038/s41589-025-02085-x

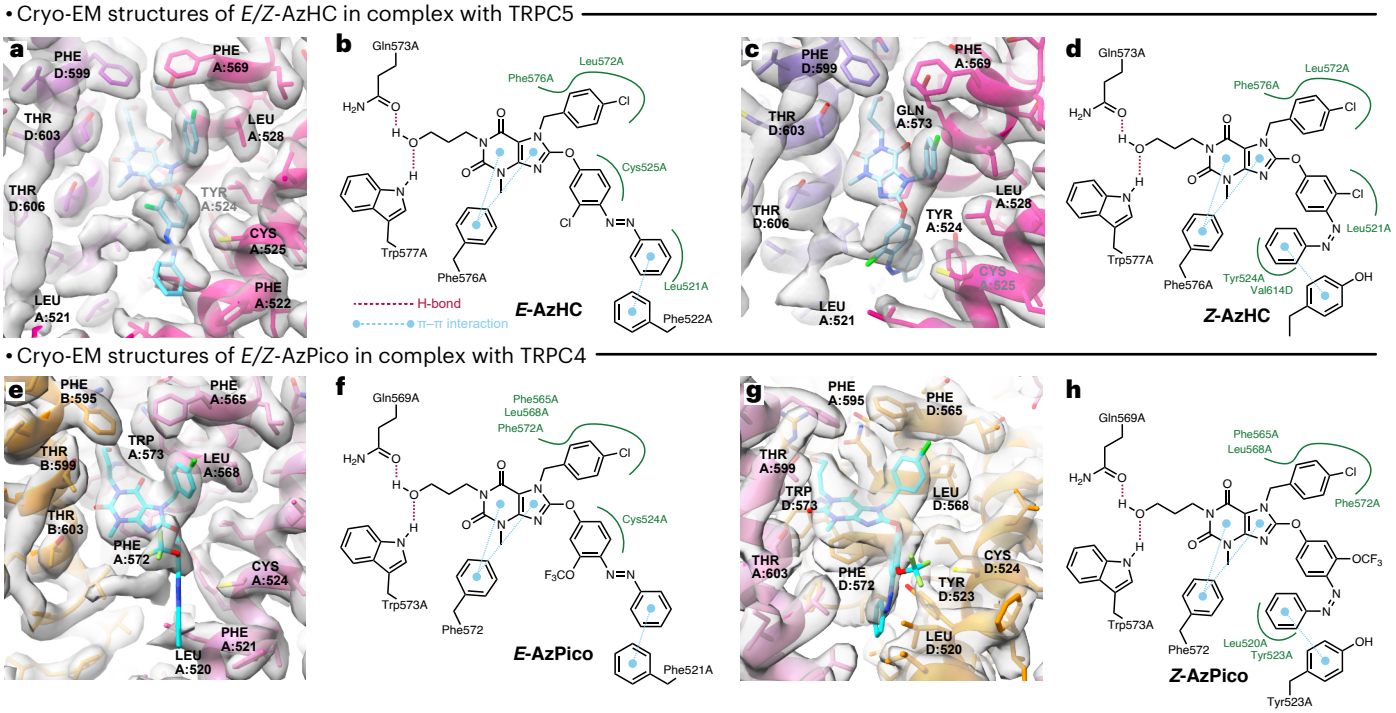


**Fig. 3 | Structures of TRPC4/5 in complex with *E*/*Z* isomers of efficacy photoswitches. a**–**d**, hTRPC5:*E*/*Z*-AzHC complexes (*E*: 2.6 Å, PDB 9G4Y, EMD-51074; *Z*: 2.9 Å, PDB 9G50, EMD-51076; $C_1$ symmetry). Note the flip of the distal azobenzene ring. **e**–**h**, $TRPC4_{DR}$:*E*/*Z*-AzPico complexes (*E*: 3.0 Å, PDB 9FXL, EMD-50850; *Z*: 3.1 Å, PDB 9FXM, EMD-50851; $C_1$ symmetry). Each complex's best-resolved xanthine-binding site is highlighted. Two-dimensional maps of ligand–protein interactions are shown.

rapidly evoked at low-nanomolar concentrations and this was rapidly photoreversible with 447-nm illumination, over many cycles (Fig. 1k). The remarkable observation that the maximum and minimum calcium signals are dose independent over a concentration range of >100-fold (from nanomolar to micromolar), even though the concentration of the agonistic *Z* isomer likewise increases >100-fold in this range, confirms it as an ideal efficacy switch (TRPC4 in Fig. 1g, l; TRPC5 in Supplementary Fig. 2 (*E*) and Supplementary Fig. 13 (*Z*)). Pleasingly, it inherits the high potency of its parent Pico145, with a 365-nm $EC_{50}$ of just 3.0 nM on TRPC4 and 4.0 nM on TRPC5 (Fig. 1n). AzHC was also a *Z*-agonistic ideal efficacy switch for TRPC5 with a 365-nm $EC_{50}$ of 6.4 nM. Excitingly, however, *Z*-AzHC was completely inactive on TRPC4 into the micromolar range (Supplementary Fig. 13). Competition assays supported that these compounds are indeed efficacy switches (Fig. 1m and Supplementary Note 1).

Taken together, these reagents are uniquely potent efficacy switches; AzPico is a photoswitchable tool addressing TRPC4; although AzPico acts on TRPC5 as well, the cellular role of TRPC4 can be tested by applying it comparatively to the TRPC5-selective AzHC, making them an outstanding reagent pair for probing these otherwise hard-to-resolve channels. Retaining the nanomolar potency of their optimized parent compounds is also a rarity among photopharmaceuticals because the extra moiety needed for photoisomerization usually sacrifices potency.

## Photomodulated electrophysiology

We next performed electrophysiological patch clamp experiments to characterize the action and specificity of channel modulation in more detail. Although its throughput is lower, electrophysiology is more powerful than FLIPR in several respects. Firstly, the nonoptical electrophysiology readout does not cause unwanted photoswitching, unlike FLIPR. Secondly, electrophysiology readouts linearly and temporally resolve ionic currents through the activated channels, unlike the delayed and attenuated fluorometric $Ca^{2+}$ influx analyses in FLIPR. Thirdly, the electrophysiology setup can use narrow-bandwidth monochromated light at any wavelength. These features allow measuring the full power of the photoswitch reagents.

We thus recorded wavelength-dependent action spectra of AzPico and AzHC under fast photoswitching in electrophysiology in TRPC4/5-expressing cells (Fig. 2 and Supplementary Fig. 14), higlighting the potential of ideal efficacy switches. For example, AzPico reversibly photomodulated TRPC4 currents over >36 consecutive cycles with a fully constant activation profile, without fatigue (Fig. 2a,b). *I*/*V* curves showed a strong activation of ion flux at best *Z* (360 nm) PSS; yet, only at nonphysiological voltages (<−80 mV or >+60 mV) could any small differences between basal activity and good *E* (440 nm) PSS be detected (Fig. 2c), making them truly off–on TRPC modulators. Reversal potentials were close to 0 mV, indicating no gross changes in the permeabilities of monovalent versus divalent cations.

As native TRPC4/5-bearing TRPC complexes are mostly heteromeric TRPC1:TRPC4 or TRPC1:TRPC5 assemblies, we tested AzPico and AzHC in cells that coexpress TRPC1 with TRPC4/5 and found photoresponse *I*/*V* curves typical for the heteromeric complexes (Supplementary Fig. 15). This supports that AzPico and AzHC give comparable chromocontrol over the TRPC1-containing heteromeric TRPC complexes to that over homomeric channels. This is noteworthy, as AM237, for example, acts strictly on TRPC5 and does not activate heteromeric TRPC1:TRPC5 (ref. 35). This flexibility favors the use of AzPico and AzHC as versatile reagents for endogenous settings (tested in Figs. 4–6).

The repeatability of on–off photocycling allowed us to extract action spectra for both (1) photoactivation (Fig. 2d,e) and (2) photodeactivation (Fig. 2f,g) in situ in live cells. Channel currents were optimally photoswitched on in a sharp wavelength range of 340–370 nm and full photoswitching off was triggered over the broad range of 400–480 nm (best: 430 nm). Such action spectra conclusively matched the highly wavelength-sensitive model expected from cell-free PSS measurements for an ideal efficacy switch (bioactivity $\propto -\log_{10}([Z]/[E])$) but mismatched the model for an affinity switch (bioactivity $\propto -\log_{10}([Z])$); this (mis)match was visible even for single-concentration data (Fig. 2h,i).

https://doi.org/10.1038/s41589-025-02085-x

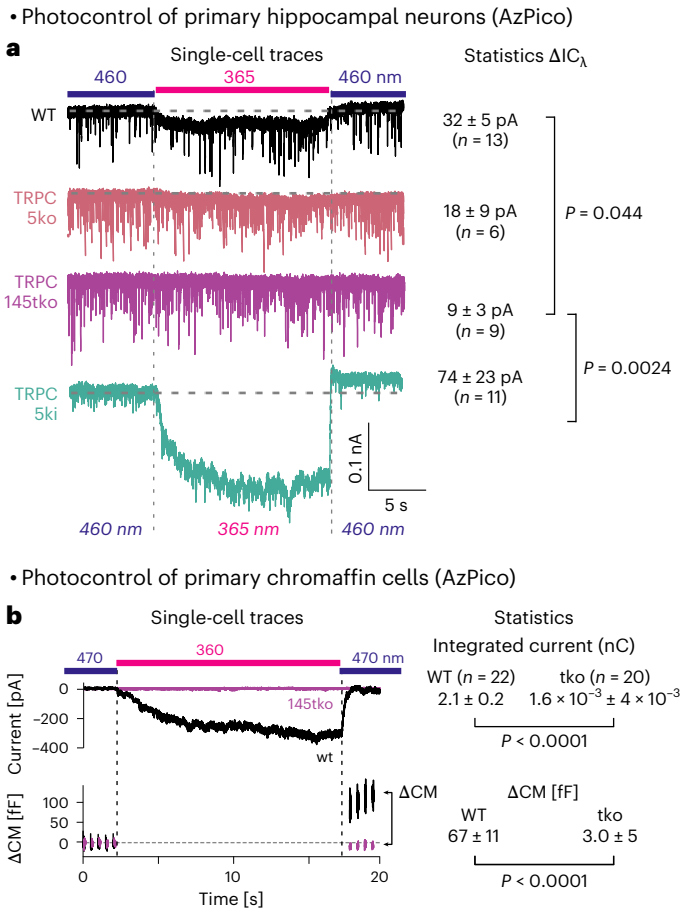


**Fig. 4 | AzPico (30 nM) photoswitchably evokes currents in primary neuronal and neuroendocrine cells. a**, Photoswitching-based current differentials $\Delta IC_\lambda$ in hippocampal neurons (currents at 365 nm relative to 460 nm). **b**, Photoswitch-based currents and net charge transfer (top) correlate with ΔCM (bottom), indicating that phototriggering of TRPC[1]/4/5 leads to exocytosis (details in Supplementary Fig. 21). Left, single-cell traces; right, group statistics.

Importantly, we recall that only the efficacy switch mechanism allows these reagents to deliver binary off–on bioactivity that is identically wavelength dependent at any concentration (Fig. 1g–i and Fig. 2h); for example, if they were classical affinity switches, even doubling their concentration would prevent photoswitching-off cell currents (Fig. 2j and Supplementary Note 1). Thus, the concentration-scan, fixed-wavelength FLIPR and the fixed-concentration, wavelength-scan electrophysiology (Fig. 1k,l, Fig. 2e,g,h and Supplementary Fig. 14) show that AzHC and AzPico are ideal efficacy switches, whose *E*/*Z*-competitive binding controls TRPC4/5 currents with exquisite wavelength sensitivity and concentration independence.

## Paired pairs of cryo-electron microscopy TRPC4/5:*E*/*Z* structures indicate activation mechanism

Single-particle cryo-electron microscopy (cryo-EM) studies of TRPC4 (refs. 59–61) and TRPC5 (refs. 62–65) have given important insights into the structures of these channels and their complexes with lipids, metals, proteins and small-molecule modulators. These include TRPC5 structures with Pico145 (ref. 64) and HC-070 (ref. 62), binding in near-identical pose to the same lipid-binding pocket, adjacent to the pore helices. However, no channel-open structures are known and all reported ligand structures are with inhibitors[36]. As AzHC and AzPico should bind with high affinity in both *E* and *Z* forms, this offered an opportunity to elucidate the structural basis of inhibitory versus activating efficacy on TRPC4/5, as well as the remarkable differential of TRPC4 activity induced by the -Cl/-OCF$_3$ swap. *E*/*Z* structure pairs could also be valuable for rational photopharmacology, as only two protein–ligand structure pairs with an azobenzene reagent bound as both *E* and *Z* isomers[49,66] are known to date.

We now studied TRPC5:*E*/*Z*-AzHC and TRPC4:*E*/*Z*-AzPico complexes by cryo-EM, hoping to acquire the 'paired pair' of both inhibited and activated structures for both channels. This work was run fully independently for TRPC4 at one site and TRPC5 at another, yet the results aligned, giving confidence in their interpretations. We could determine all four structures at high resolution (human (h)TRPC5:*E*-AzHC, 2.6 Å; hTRPC5:*Z*-AzHC, 2.9 Å; TRPC4$_{DR\ (Danio\ rerio)}$:*E*-AzPico, 3.0 Å; TRPC4$_{DR}$:*Z*-AzPico, 3.1 Å) without imposing symmetry during data processing (Fig. 3, Supplementary Figs. 16–20, Supplementary Tables 4–7 and Supplementary Videos 1–4). We used 365 nm for *Z* ligand structures and dark or 440 nm for *E* structures; furthermore, we excluded DTT from all buffers to avoid diazene reduction.

Supplementary Note 4 contains full details of the structural biology results. Briefly, *E*/*Z*-AzHC/AzPico could be built into the expected lipid-binding or xanthine-binding site, with near-identical positions to that of Pico145 (ref. 64) for the conserved ligand portion and differences between the *E* and *Z* isomers only at the azobenzene. For example, the distal ring of *E*-AzHC is projected outward to make a $\pi$–$\pi$ interaction with Phe522 of TRPC5, whereas, in *Z*-AzHC, it folds deeply inward to make a $\pi$–$\pi$ interaction with Y524; AzPico behaves similarly on TRPC4 (Fig. 3 and Supplementary Figs. 4–6). Most protein residues in the ligand-binding site are in similar positions in the *E*/*Z* structures; the exceptions are that, for hTRPC5, Phe520 is flipped 'in' or 'out' depending on whether the antagonistic *E* or agonistic *Z* isomer is bound (Supplementary Fig. 4b), while, in TRPC4$_{DR}$, the cognate Phe521 is much less shifted, although its neighboring L520 is notably displaced (Supplementary Videos 1–4). All *E* and *Z* structures had the channel pore closed (potential reasons for this in Supplementary Figs. 5–7); thus, caution in interpreting the agonist structures is needed. Nevertheless, these data offer structural insight into how closely related xanthines can have opposite effects on TRPC4/5 function (that is, inhibition versus activation).

With these binding modes confirmed, we tested whether the selective activation of TRPC5 but not TRPC4 by *Z*-AzHC could be the result of the single-amino-acid difference in their binding sites (Val579 in TRPC5 versus Ile575 in TRPC4 at the cognate position). However, neither the Val579Ile nor the Ile575Val substitution in TRPC5 and TRPC4, respectively, changed their activity profiles for *E*/*Z*-AzHC or for control activator AM237. This suggests that the basis for *Z*-AzHC's TRPC5-selective activation is more complex than the immediate residues it contacts (Supplementary Note 4).

## Photoswitching endogenous TRPC4/5 in primary cells to photoreversibly actuate cell function

We next moved to test whether AzPico can directly chromocontrol endogenous TRPC4/5, using autaptic hippocampal neurons (neurons cultured in isolation, which only make synapses back onto themselves, as a model for simultaneously monitoring presynaptic and postsynaptic responses). The 365/460-nm cycles reversibly activated inward currents in wild-type (WT) neurons, just as was seen in heterologously TRPC4/5-(over)expressing HEK cells (Fig. 2). These WT neurons consist of a fraction of cells expressing TRPC channels that can be directly activated by AzPico plus about 50% of neurons that do not express TRPC channels[67]. Matching expectations, average currents were larger when acquired exclusively from TRPC5-bearing cells (5ki), strongly depressed with TRPC5 single knockout (5ko) and almost abolished with TRPC1/C4/C5 triple knockout (145tko), supporting that TRPC[1]4/5 channels are the central contributor to AzPico's photomodulation of membrane conductance (Fig. 4a)[68]. This shows that AzPico can optically control the activity of native TRPC[1/4/]5 channels in primary nerve cells without channel overexpression.

https://doi.org/10.1038/s41589-025-02085-x

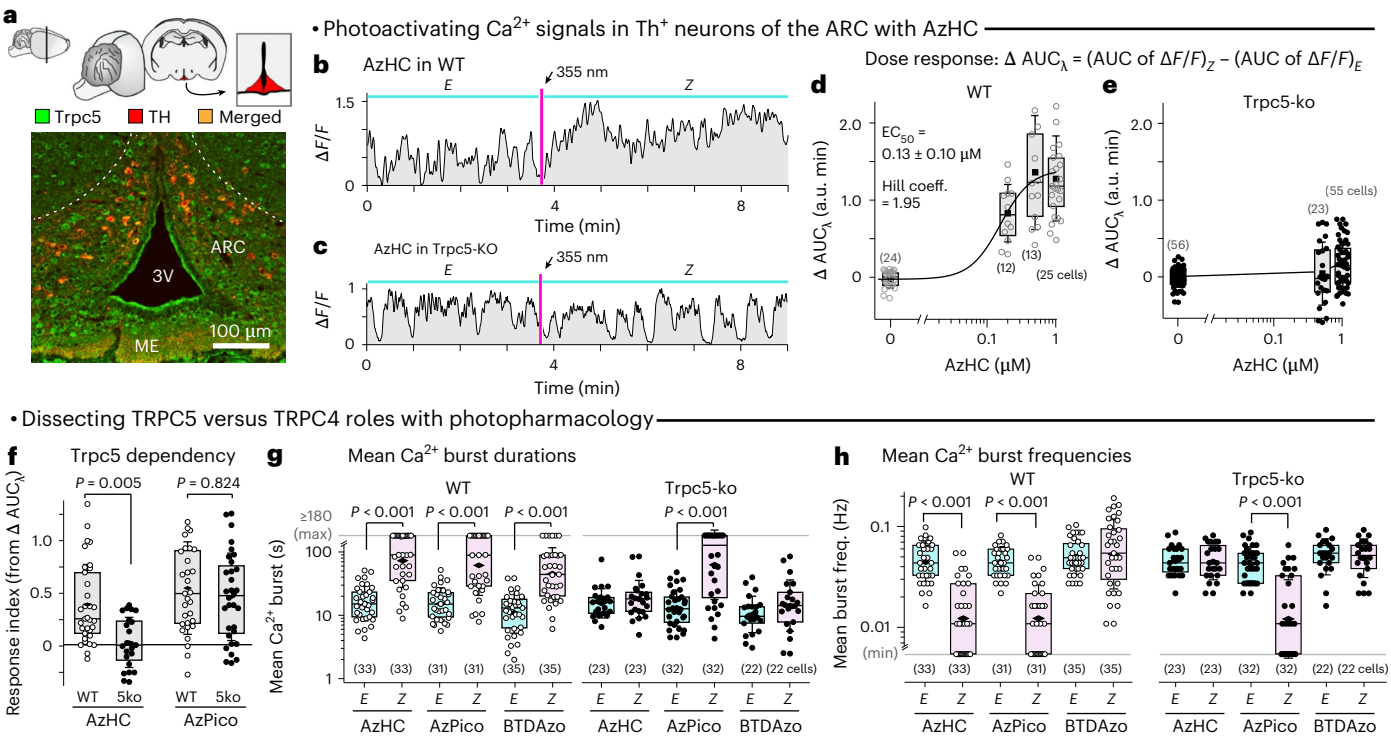


**Fig. 5 | AzHC and AzPico are potent photoswitchable activators of TRPC-dependent $Ca^{2+}$ responses in mouse hypothalamus. a**, Coronal brain slice: cartoon with ARC region in red and microscopy image with Trpc5 immunostained in green and $Th^+$ neurons in red (representative image from $n = 4$ mice). **b**–**h**, $Ca^{2+}$ responses in $Th^+$ neurons of Th-GCaMP6f (WT) or Th-GCaMP6f-ΔTrpc5 (Trpc5-ko or 5ko) mice. **b**,**c**, Single-cell $Ca^{2+}$ traces before (*E*) and after (*Z*) a 355-nm pulse. **d**,**e**, $\Delta AUC_\lambda$, light dependency of the AUC as acquired in **b**,**c**. **f**, AzHC only chromocontrols TRPC5-dependent $Ca^{2+}$ responses; AzPico can chromocontrol $Ca^{2+}$ responses by another route (likely TRPC4). **g**,**h**, mean $Ca^{2+}$ burst durations and frequencies in WT and 5ko upon *E*→*Z* photoswitching. AzHC/AzPico, 500 nM (except in dose–response study); BTDazo, 10 µM. In **d**–**h**, each point represents one cell with *n* cells per group. Box plots show the interquartile ranges, median (line), mean (black rhombus) and s.d. (whiskers). In **f**–**h**, statistical analysis was conducted using a Kruskal–Wallis analysis of variance (ANOVA) and Dunn's *P* values are shown. In **g**,**h**, if no *P* value is indicated, then the data were not significantly different between the *E* and *Z* isomers of AzHC or BTDAzo ($P = 0.052$–$0.999$; **g**, Kruskal–Wallis ANOVA: $\chi^2(11) = 132.71744$, $P < 0.0001$; **h**, Kruskal–Wallis ANOVA: $\chi^2(11) = 142.9224$, $P < 0.0001$). Min–max values and all other details are provided in Supplementary Fig. 22 (full legend in Supplementary Information).

We then tested the photopharmacology of AzPico in isolated primary chromaffin cells (the neuroendocrine cells in the adrenal gland that secrete adrenaline by exocytosis in response to electrical activation and functionally express TRPC1/4/5 channels)[69]. The 360-nm illumination of AzPico photoreversibly triggered robust inward currents that caused an increase in membrane capacitance (CM) in WT cells, indicative of exocytosis (Fig. 4b). Neither response was observed in 145tko cells, confirming the TRPC specificity of this photopharmacology. By supporting that direct activation of endogenous TRPC channels in chromaffin cells can trigger exocytosis, this again suggests how AzPico may be used to exert functional control over endogenous biology (here, for optically controlled release of adrenaline).

## TRPC4/5 photoswitches are effective in tissue slices and can reveal channel-specific biology

We believed that AzHC and AzPico's efficacy switch mechanism and high potency should make them effective chromocontrol reagents for deeper tissues and moved to test it. The hypothalamic arcuate nucleus (ARC) (Fig. 5a) is a signaling center in the brain where most dopamine ($Th^+$) neurons are known to express TRPC5, which contributes not only to spontaneous oscillatory burst-firing activity and $Ca^{2+}$ burst responses[34] but also to sustained activation following stimulation with the hormone prolactin (a mechanism of reproductive signaling that has been conserved for >300 million years)[12,34]. The temporal distinction between these activation modes is striking and suggests the possibility of using either AzHC or AzPico as a time-resolved TRPC5 probe. However, we remain ignorant even of whether the most closely related congener TRPC4 has a role in this circuitry; hence, we were particularly drawn to apply these reagents comparatively, hoping that their intersecting C4/C5 selectivities could deliver new information about TRPC4 biology in endogenous systems.

We therefore took 275-µm-thick mouse brain slices through the dorsomedial ARC (Fig. 5a) and imaged the $Ca^{2+}$ indicator GCaMP6f in $Th^+$ neurons while photoswitching AzHC or AzPico to study TRPC[4]/5 photoactuation in situ. $Ca^{2+}$ influx should be seen across several independent parameters: from time-resolved aspects such as longer $Ca^{2+}$ burst durations and lower $Ca^{2+}$ burst frequency to simply larger areas under the curve of the fluorescent $Ca^{2+}$ signal (AUC), which translate into a 'response index' > 1 (details in Supplementary Fig. 22). Pleasingly, we again found that AzHC and AzPico can strongly photoswitch $Ca^{2+}$ responses at endogenous TRPC levels by all these metrics. A single ≥23-ms pulse of 355-nm light (*E*→*Z*) induced dramatically sustained high-$Ca^{2+}$ signals lasting up to ≥3 min (42% of cells; Fig. 5b,d,g,h). TRPC5 was sufficient for this signal, as TRPC5-knockout slices did not respond to AzHC photoswitching (Fig. 5c,e). However, *Z*-AzPico $Ca^{2+}$ photoresponses were maintained despite TRPC5 knockout, providing functional evidence for a role of TRPC4 or TRPC1/C4 in the $Ca^{2+}$ response in dorsomedial $Th^+$ neurons of the ARC (Fig. 5f–h and Supplementary Fig. 22c,d), which can now be further explored[12].

This discovery underscores the utility of this pair of photoswitches for deconvoluting the roles of TRPC4 from TRPC5. We also stress how important it was for these studies that the reagents were high-potency and ideal efficacy photoswitches. This allowed internally baselining signals after compound application (to overcome

https://doi.org/10.1038/s41589-025-02085-x

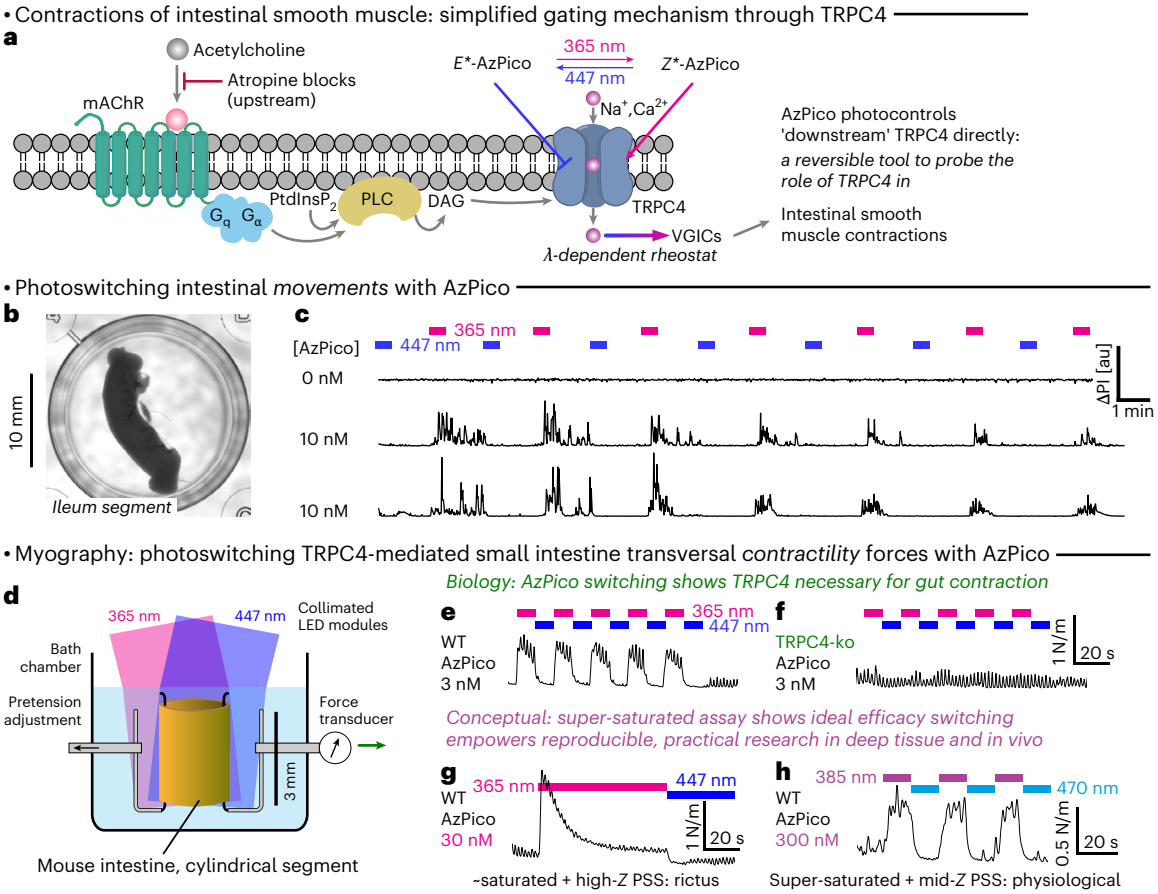


**Fig. 6 | AzPico chromocontrol of intestinal contractility shows the key role of TRPC4 and power of ideal efficacy switching. a**, Simplified molecular mechanism for TRPC4-dependent intestinal contractility[75], which is directly testable using AzPico (*E**/*Z** indicate *E*/*Z*-rich-PSSs). **b**,**c**, Intestinal segments (mouse ileum) whose motility was blocked by atropine but treated with AzPico were driven into phases of fast macroscopic motions by UV photoswitching (longitudinal and ring muscle contractility) and then returned to immobility by blue light, reversibly over many cycles (Supplementary Video 5). **d**–**f**, Physiological-like ring contractility is reversibly stimulated and suppressed by alternating UV and blue illumination of segments treated with AzPico in a TRPC4-dependent manner. **g**,**h**, The ideal efficacy switch paradigm allows fully reproducible control of deep tissue bioactivity, by leveraging the saturation of dose and photon flux (hard to titrate) but the selection of wavelength (easy to choose) (Supplementary Fig. 23) (full legend in Supplementary Information).

expression heterogeneity) and then photoswitching activity on from zero background at a precisely defined time in a fully reproducible wavelength-dependent manner (all needed for reliable statistics). Temporally modulated studies beyond the scope of this report are already underway, motivated by the xanthines' sustained (low-frequency) $Ca^{2+}$ bursts that contrast the photoswitchable TRPC5 activator BTDazo (burst frequency barely affected; Fig. 5h). This points to a rich interplay of pharmacology and spatiotemporally resolved biology in complex tissues, which photoswitchable reagents are uniquely poised to tackle.

## Photoswitching tissue-level physiology via TRPC4-based chromocontrol of intestinal motility

After observing chromocontrol in thin tissue slices by microscopy, we next tested for photoactuation of macroscopic downstream processes in thick tissue sections of the intestine. Landmark papers by Freichel[70] and Zholos[16] used irreversible suppression assays to suggest that TRPC4 activation, downstream from muscarinic acetylcholine receptors (mAChRs, the target of atropine), should be a critical component controlling small intestine peristalsis. Intestinal segment contractions are macroscopically coordinated oscillatory motions overlaid on a 'tonic' baseline contractile force. A subthreshold oscillatory pacemaker potential is amplified by mAChR through phospholipase C and TRPC4 activation to surpass the threshold potential of voltage-gated $Ca^{2+}$ channels, leading to peristaltic contractions (Fig. 6a). We, therefore, expected that direct TRPC4 activation by *Z*-AzPico might hijack the pacemaker signal to drive oscillatory contractility, even with upstream signaling by mAChR blocked, and aimed to test this so as to directly elucidate the role of TRPC4 activation in intestinal contractility in endogenous tissues.

We took fresh 8–12-mm-long segments of mouse small intestine (jejuneal and ileal), added low atropine concentrations (300 nM) to paralyze their spontaneous motility and monitored their contractility by macroscopic video imaging while photoswitching AzPico (Fig. 6b). Indeed, even with just 10 nM AzPico, ultraviolet (UV) illumination initiated vigorous motions that were stopped rapidly by applying 447-nm light and then restarted with UV; the on–off chromocontrol could be cycled many times (Fig. 6c and Supplementary Video 5). No intestinal light responses were evident without AzPico and, highlighting the tissue-specificity involved, AzPico-treated colon segments also had no photoresponse.

We next analyzed intestinal contractility quantitatively, monitoring contractile muscle force in 3-mm-long ileal or jejuneal segments by myography during AzPico photoswitching with UV and blue light (Fig. 6d). With moderate AzPico concentrations (for example, 3 nM), 365-nm UV illumination not only increased tonic forces but also doubled oscillatory forces (1.9×) without changing oscillatory frequency, indicating that *Z*-AzPico 'rides' the circuit to drive typical contractility. Basal tension was then restored under 447-nm light and 365/447-nm cycling could be repeated many times (Fig. 6e). We assigned this intestinal chromocontrol to TRPC4 as segments of TRPC4-deficient mice[71] never responded to *E*/*Z*-AzPico (Fig. 6f), while tonic and oscillatory

force photoresponses in TRPC5-deficient mice were indistinguishable from those in matched control mice.

Our findings, thus, support that TRPC4 activation is both necessary and sufficient to convert subthreshold oscillatory signals into effective peristaltic motility in the small intestine. On an applied level, the AzPico-induced, optically tunable reactivation of atropine-paralyzed intestinal segments suggests potential experimental therapies to treat intestinal motility insufficiency conditions such as toxic or postoperative paralytic ileus. On a more conceptual level, the full and rapid photoreversibility of both gross motility and myographic readouts, assessed on the tissue level in WT samples, gives high confidence in the molecular TRPC4 specificity of intestinal contractility. We stress, however, that this simple and direct result is only possible for the ideal efficacy photoswitch, whereas classical high-affinity compounds such as EA or Pico145 practically cannot be washed out; hence, internally baselined, reversible experimentation without fatigue-based rundown or gross toxicity[72] was previously impossible. We also highlight that we used a small-molecule photoswitch to elucidate a target through hypothesis-driven research, instead of creating and using a photoswitch after target identification.

However, given the in vivo potential of ideal efficacy photoswitches, we are certain that this will not be the last such case. A practical example of the value of chromocontrol that such photoswitches finally enable is illustrative. Our protocols converged to the use of 365 nm for high-completion *E*→*Z* switching and best channel activation; however, with moderate to high concentrations of AzPico (30 nM), this resulted in rictus-like intestinal tensioning and rundown, presumably through overstimulation (Fig. 6g). This seems to be a regular biological situation, whereby a desired, physiological effect is only reached when a target protein is partially but not fully stimulated. This overstimulation could be avoided in a classical way by titrating AzPico concentrations down to ~3 nM (Supplementary Information) but ideal efficacy switching should allow the much simpler workaround of merely changing the illumination wavelength. To test the ideal model in Fig. 1g–i as stringently as possible, we saturated tissues using 300 nM AzPico but adopted 385 nm instead for UV illumination (also applied as saturating illumination). This 20-nm wavelength shift perfectly and reproducibly drove only partial channel activation, giving the physiology-like oscillatory intestinal contractions we sought (Fig. 6h). We feel that using both saturating ligand concentration and saturating light fluence is key for avoiding the practical irreproducibilities of 'tuned compound and light dosing' that is required for affinity switches to operate and illustrates why a paradigm shift to ideal efficacy photoswitching can empower deep tissue or in vivo research, even for targets (for example, TRPC4/5) that are nonlinearly responsive and have time-dependent and dose-dependent bioactivity.

## Discussion

We rationally developed AzHC and AzPico as ideal efficacy photoswitches for TRPC[4]/5. Their photoisomerization flips them between *E* inverse agonists and *Z* agonists, with both forms having excellent binding affinity, resulting in a pair of lit-active low-nanomolar-potency tools that can be used together to elucidate TRPC5-selective or TRPC4-selective biology. To date, there have only been two reports of protein–ligand structures where both *E* and *Z* isomers of the same azobenzene reagent were bound[49,66]; we now report two more, with both TRPC4 and TRPC5 *E*/*Z* structure pairs, which will help progress design rules for efficacy switches on other targets. Unlike nearly all photopharmaceuticals, the bioactivity of AzHC and AzPico is fully determined by the illumination wavelength used but not their concentration. This makes them suitable for reliable and reproducible chromocontrol across diverse model systems, from overexpression in HEK cells to endogenous expression in primary neurons, adrenalin-secreting cells, brain slices and intact segments of intestine, where they elegantly support a hypothesis for TRPC4-dependent contractility.

Importantly for the TRPC field, the tissue-level chromocontrol by nanomolar AzPico and AzHC marks these reagents as exceptionally effective optical tools for precisely and reversibly manipulating endogenous TRPC biology[17] in situ. Their likely applications, thus, stretch far beyond the muscular and neuronal applications shown here, toward elucidating TRPC4/5's rich and largely still cryptic biology. Lastly, the rapid macroscopic photoswitchability of AzPico's downstream secondary and tertiary effects (that is, not only ion flux but also integration in the native cascade controlling tissue-scale muscle movement) is highly unusual if not unique in photopharmacology (Fig. 6).

For biology and chemistry in general, we showed that the ideal efficacy photoswitching paradigm can be rationally chemically designed and rationally biologically exploited to achieve robust high-precision control of endogenous systems that is purely directed by light rather than drug dosing and distribution. This feature combination makes it suited excellently for deep tissue and in vivo work. We introduced some general biological target considerations and general chemical design concepts to ground the wider introduction of efficacy photoswitching (Supplementary Note 2). Of course, the pharmacological requirement to design an efficacy photoswitch is that an efficacy 'cliff' should be plausible and this is not the case for many families of highly active drugs. For example, substrate or cosubstrate mimics that inhibit enzymes in their active site cannot be made to instead agonize enzyme activity while still binding; thus, they are not convertible into efficacy photoswitches. By contrast, allosteric modulatory sites (which, in many cases, are already known to allow both positive and negative allosteric modulation) seem ideally feasible candidates from the pharmacological perspective. Furthermore, our perception is that this target-based design opportunity is closely matched to real, biologically based needs. We define 'poised targets' as being those proteins that need to rapidly and spatiotemporally modulate their functions to support life (ion channels, receptors, sensory or signaling integrators, etc.). We perceive that such poised targets are most likely to be addressable by the efficacy switch paradigm, as they are often evolved to allow small modulators or ligands to bias their activity. Moreover, we perceive that these are also the targets that most urgently require modulatory reagents delivering high spatiotemporal resolution across the scales even to in vivo settings (as efficacy photoswitch reagents promise) to understand their endogenous biology. That match of need to opportunity is not accidental; it simply reflects how biology has evolved and perfected its own ligand-based or protein-based regulatory mechanisms to operate in complex environments. Accordingly, efficacy photoswitching can be an ideal way to harness this potential to the fullest.

Lastly, we encourage chemists to take up awareness of this possibility, to rigorously test for it even where it was not a design aim[29,54,55] and to work toward rationally using the efficacy photoswitching paradigm to generate a cornucopia of reagents that are more in vivo competent rather than remaining locked to affinity photoswitching approaches. We foresee that such efficacy photoswitches can unlock a new era for chromocontrolled biology, in ways that not only deeply impact chemical or cell culture proof-of-principle studies but translate seamlessly across to basic physiology and medical research, enabling researchers to noninvasively probe and modulate endogenous pathways in deep tissues and in vivo.

## Data and material availability

All data needed to evaluate the conclusions in the paper are present in the paper and/or the Supplementary Information. Data were also deposited and are freely available on bioRxiv[73] and figshare[74]. Cryo-EM structures were deposited to the Protein Data Bank and EM Data Bank under the following accession codes: TRPC4DR:*E*-AzPico, 3.0 Å, PDB 9FXL, EMD-50850; TRPC4DR:*Z*-AzPico, 3.1 Å, PDB 9FXM, EMD-50851; hTRPC5:*E*-AzHC, 2.6 Å, PDB 9G4Y, EMD-51074; hTRPC5:*Z*-AzHC, 2.9 Å, PDB 9G50, EMD-51076.

### Reporting summary

Further information on research design is available in the Nature Portfolio Reporting Summary linked to this article.

## Online content

Any methods, additional references, Nature Portfolio reporting summaries, source data, extended data, supplementary information, acknowledgements, peer review information; details of author contributions and competing interests; and statements of data and code availability are available at https://doi.org/10.1038/s41589-025-02085-x.

## References


1. Clapham, D. E. TRP channels as cellular sensors. *Nature* **426**, 517–524 (2003).
2. Flockerzi, V. & Nilius, B. in *Mammalian Transient Receptor Potential (TRP) Cation Channels* (eds Nilius, B. & Flockerzi, V.) (Springer, 2014).
3. Kaneko, Y. & Szallasi, A. Transient receptor potential (TRP) channels: a clinical perspective. *Br. J. Pharmacol.* **171**, 2474–2507 (2014).
4. Koivisto, A.-P., Belvisi, M. G., Gaudet, R. & Szallasi, A. Advances in TRP channel drug discovery: from target validation to clinical studies. *Nat. Rev. Drug. Discov.* **21**, 41–59 (2022).
5. Zhang, M. et al. TRP (transient receptor potential) ion channel family: structures, biological functions and therapeutic interventions for diseases. *Signal Transduct. Target. Ther.* **8**, 1–38 (2023).
6. Clapham, D. E., Runnels, L. W. & Strübing, C. The TRP ion channel family. *Nat. Rev. Neurosci.* **2**, 387–396 (2001).
7. Zholos, A. V. TRPC5. in *Mammalian Transient Receptor Potential (TRP) Cation Channels* (eds Nilius, B. & Flockerzi, V.) (Springer, 2014).
8. Freichel, M., Tsvilovskyy, V. & Camacho-Londoño, J. E. in *Mammalian Transient Receptor Potential (TRP) Cation Channels* (eds Nilius, B. & Flockerzi, V.) (Springer, 2014).
9. Sadler, K. E. et al. Transient receptor potential canonical 5 mediates inflammatory mechanical and spontaneous pain in mice. *Sci. Transl. Med.* **13**, eabd7702 (2021).
10. Bernal, L. et al. Odontoblast TRPC5 channels signal cold pain in teeth. *Sci. Adv.* **7**, eabf5567 (2021).
11. Koivisto, A.-P., Voets, T., Iadarola, M. J. & Szallasi, A. Targeting TRP channels for pain relief: A review of current evidence from bench to bedside. *Curr. Opin. Pharmacol.* **75**, 102447 (2024).
12. Blum, T. et al. Trpc5 deficiency causes hypoprolactinemia and altered function of oscillatory dopamine neurons in the arcuate nucleus. *Proc. Natl Acad. Sci. USA* **116**, 15236–15243 (2019).
13. Riccio, A. et al. Decreased anxiety-like behavior and Gαq/11-dependent responses in the amygdala of mice lacking TRPC4 channels. *J. Neurosci.* **34**, 3653–3667 (2014).
14. Riccio, A. et al. Essential role for TRPC5 in amygdala function and fear-related behavior. *Cell* **137**, 761–772 (2009).
15. Zhou, Y. et al. A small-molecule inhibitor of TRPC5 ion channels suppresses progressive kidney disease in animal models. *Science* **358**, 1332–1336 (2017).
16. Dryn, D. O., Melnyk, M. I., Bon, R. S., Beech, D. J. & Zholos, A. V. Pico145 inhibits TRPC4-mediated mICAT and postprandial small intestinal motility. *Biomed. Pharmacother.* **168**, 115672 (2023).
17. Li, Y. et al. Loss of transient receptor potential channel 5 causes obesity and postpartum depression. *Cell* **187**, 4176–4192 (2024).
18. Dietrich, A., Fahlbusch, M. & Gudermann, T. Classical transient receptor potential 1 (TRPC1): channel or channel regulator? *Cells* **3**, 939–962 (2014).
19. Bon, R. S. & Beech, D. J. In pursuit of small molecule chemistry for calcium-permeable non-selective TRPC channels—mirage or pot of gold? *Br. J. Pharmacol.* **170**, 459–474 (2013).
20. Sharma, S. & Hopkins, C. R. Review of transient receptor potential canonical (TRPC5) channel modulators and diseases. *J. Med. Chem.* **62**, 7589–7602 (2019).
21. Ratnayake, R., Covell, D., Ransom, T. T., Gustafson, K. R. & Beutler, J. A. Englerin A, a selective inhibitor of renal cancer cell growth, from *Phyllanthus engleri*. *Org. Lett.* **11**, 57–60 (2009).
22. Akbulut, Y. et al. (−)-Englerin A is a potent and selective activator of TRPC4 and TRPC5 calcium channels. *Angew. Chem. Int. Ed.* **54**, 3787–3791 (2015).
23. Radtke, L. et al. Total synthesis and biological evaluation of (−)-englerin A and B: synthesis of analogues with improved activity profile. *Angew. Chem. Int. Ed.* **50**, 3998–4002 (2011).
24. Just, S. et al. Treatment with HC-070, a potent inhibitor of TRPC4 and TRPC5, leads to anxiolytic and antidepressant effects in mice. *PLoS ONE* **13**, e0191225 (2018).
25. Yu, M. et al. Discovery of a potent and selective TRPC5 inhibitor, efficacious in a focal segmental glomerulosclerosis model. *ACS Med. Chem. Lett.* **10**, 1579–1585 (2019).
26. Curcic, S., Tiapko, O. & Groschner, K. Photopharmacology and opto-chemogenetics of TRPC channels-some therapeutic visions. *Pharmacol. Ther.* **200**, 13–26 (2019).
27. Frank, J. A. et al. Photoswitchable fatty acids enable optical control of TRPV1. *Nat. Commun.* **6**, 7118 (2015).
28. Stein, M., Breit, A., Fehrentz, T., Gudermann, T. & Trauner, D. Optical control of TRPV1 channels. *Angew. Chem. Int. Ed.* **52**, 9845–9848 (2013).
29. Lam, P.-Y. et al. TRPswitch—a step-function chemo-optogenetic ligand for the vertebrate TRPA1 channel. *J. Am. Chem. Soc.* **142**, 17457–17468 (2020).
30. Tiapko, O. et al. Lipid-independent control of endothelial and neuronal TRPC3 channels by light. *Chem. Sci.* **10**, 2837–2842 (2019).
31. Leinders-Zufall, T. et al. PhoDAGs enable optical control of diacylglycerol-sensitive transient receptor potential channels. *Cell Chem. Biol.***25**, 215–223 (2018).
32. Leinders-Zufall, T. et al. A diacylglycerol photoswitching protocol for studying TRPC channel functions in mammalian cells and tissue slices. *STAR Protoc.* **2**, 100527 (2021).
33. Lichtenegger, M. et al. An optically controlled probe identifies lipid-gating fenestrations within the TRPC3 channel. *Nat. Chem. Biol.* **14**, 396–404 (2018).
34. Müller, M. et al. BTDAzo: a photoswitchable TRPC5 channel activator. *Angew. Chem. Int. Ed.* **61**, e202201565 (2022).
35. Minard, A. et al. Potent, selective, and subunit-dependent activation of TRPC5 channels by a xanthine derivative. *Br. J. Pharmacol.* **176**, 3924–3938 (2019).
36. Bauer, C. C. et al. Xanthine-based photoaffinity probes allow assessment of ligand engagement by TRPC5 channels. *RSC Chem. Biol.* **1**, 436–448 (2020).
37. Fuchter, M. J. On the promise of photopharmacology using photoswitches: a medicinal chemist's perspective. *J. Med. Chem.* **63**, 11436–11447 (2020).
38. Thorn-Seshold, O. & Meiring, J. C. M. in *Microtubules: Methods and Protocols* (ed. Inaba, H.) (Springer, 2022).
39. Thorn-Seshold, O. in *Molecular Photoswitches: Chemistry, Properties, and Applications* (ed. Pianowski, Z. L.) (Wiley, 2022).
40. Hüll, K., Morstein, J. & Trauner, D. In vivo photopharmacology. *Chem. Rev.* **118**, 10710–10747 (2018).
41. Colquhoun, D. Binding, gating, affinity and efficacy: the interpretation of structure-activity relationships for agonists and of the effects of mutating receptors. *Br. J. Pharmacol.* **125**, 923–947 (1998).
42. Agnetta, L. et al. A photoswitchable dualsteric ligand controlling receptor efficacy. *Angew. Chem. Int. Ed.* **56**, 7282–7287 (2017).

43. Gómez-Santacana, X. et al. A toolbox of molecular photoswitches to modulate the CXCR3 chemokine receptor with light. *Beilstein J. Org. Chem.* **15**, 2509–2523 (2019).
44. Steinmüller, S. A. M., Tutov, A., Hislop, J. N. & Decker, M. Bridging the binding sites 2.0: photoswitchable dualsteric ligands for the cannabinoid 2 receptor. *ACS Chem. Neurosci.* **14**, 3737–3744 (2023).
45. Hansen, M. J., Hille, J. I. C., Szymanski, W., Driessen, A. J. M. & Feringa, B. L. Easily accessible, highly potent, photocontrolled modulators of bacterial communication. *Chem* **5**, 1293–1301 (2019).
46. Gerwe, H., He, F., Pottie, E., Stove, C. & Decker, M. Enlightening the "spirit molecule": photomodulation of the 5-HT2A receptor by a light-controllable N,N-dimethyltryptamine derivative. *Angew. Chem. Int. Ed.* **61**, e202203034 (2022).
47. Riefolo, F. et al. Optical control of cardiac function with a photoswitchable muscarinic agonist. *J. Am. Chem. Soc.* **141**, 7628–7636 (2019).
48. Gómez-Santacana, X. et al. Photoswitching the efficacy of a small-molecule ligand for a peptidergic GPCR: from antagonism to agonism. *Angew. Chem. Int. Ed.* **57**, 11608–11612 (2018).
49. Arkhipova, V. et al. Structural aspects of photopharmacology: insight into the binding of photoswitchable and photocaged inhibitors to the glutamate transporter homologue. *J. Am. Chem. Soc.* **143**, 1513–1520 (2021).
50. Westphal, M. V. et al. Synthesis of photoswitchable Δ9-tetrahydrocannabinol derivatives enables optical control of cannabinoid receptor 1 signaling. *J. Am. Chem. Soc.* **139**, 18206–18212 (2017).
51. Panarello, S., Rovira, X., Llebaria, A. & Gómez-Santacana, X. Photopharmacology of G-protein-coupled receptors. In *Molecular Photoswitches: Chemistry, Properties, and Applications* (ed. Pianowski, Z. L.) (Wiley, 2022).
52. Bahamonde, M. I. et al. Photomodulation of G protein-coupled adenosine receptors by a novel light-switchable ligand. *Bioconjug. Chem.* **25**, 1847–1854 (2014).
53. Cao, Y. et al. Photo-clenbuterol: optical control of β2-adrenergic receptor signaling by photoswitchable ligand efficacy. *J. Med. Chem.* **68**, 12911–12924 (2025).
54. Morstein, J. et al. Optical control of sphingosine-1-phosphate formation and function. *Nat. Chem. Biol.* **15**, 623–631 (2019).
55. Yue, L. et al. Robust photoregulation of GABAA receptors by allosteric modulation with a propofol analogue. *Nat. Commun.* **3**, 1095 (2012).
56. Morstein, J. et al. Optical control of lysophosphatidic acid signaling. *J. Am. Chem. Soc.* **142**, 10612–10616 (2020).
57. Chenard, B. & Gallaschun, R. Substituted xanthines and methods of use thereof. WIPO patent WO2014143799A3 (2014).
58. Rubaiy, H. N. et al. Picomolar, selective, and subtype-specific small-molecule inhibition of TRPC1/4/5 channels. *J. Biol. Chem.* **292**, 8158–8173 (2017).
59. Vinayagam, D. et al. Electron cryo-microscopy structure of the canonical TRPC4 ion channel. *eLife* **7**, e36615 (2018).
60. Duan, J. et al. Structure of the mouse TRPC4 ion channel. *Nat. Commun.* **9**, 3102 (2018).
61. Vinayagam, D. et al. Structural basis of TRPC4 regulation by calmodulin and pharmacological agents. *eLife* **9**, e60603 (2020).
62. Song, K. et al. Structural basis for human TRPC5 channel inhibition by two distinct inhibitors. *eLife* **10**, e63429 (2021).
63. Won, J. et al. Molecular architecture of the $G\alpha_i$-bound TRPC5 ion channel. *Nat. Commun.* **14**, 2550 (2023).
64. Wright, D. J. et al. Human TRPC5 structures reveal interaction of a xanthine-based TRPC1/4/5 inhibitor with a conserved lipid binding site. *Commun. Biol.* **3**, 704 (2020).
65. Duan, J. et al. Cryo-EM structure of TRPC5 at 2.8-Å resolution reveals unique and conserved structural elements essential for channel function. *Sci. Adv.* **5**, eaaw7935 (2019).
66. Pospich, S. et al. Cryo-EM resolves molecular recognition of an optojasp photoswitch bound to actin filaments in both switch states. *Angew. Chem. Int. Ed.* **60**, 8678–8682 (2021).
67. Schwarz, Y. et al. TRPC channels regulate $Ca^{2+}$-signaling and short-term plasticity of fast glutamatergic synapses. *PLoS Biol.* **17**, e3000445 (2019).
68. Bröker-Lai, J. et al. Heteromeric channels formed by TRPC1, TRPC4 and TRPC5 define hippocampal synaptic transmission and working memory. *EMBO J.* **36**, 2770–2789 (2017).
69. Bröker-Lai, J. et al. TRPC5 controls the adrenaline-mediated counter regulation of hypoglycemia. *EMBO J.* **43**, 5813–5836 (2024).
70. Tsvilovskyy, V. V. et al. Deletion of *TRPC4* and *TRPC6* in mice impairs smooth muscle contraction and intestinal motility in vivo. *Gastroenterology* **137**, 1415–1424 (2009).
71. Freichel, M. et al. Lack of an endothelial store-operated $Ca^{2+}$ current impairs agonist-dependent vasorelaxation in $TRP4^{-/-}$ mice. *Nat. Cell Biol.* **3**, 121–127 (2001).
72. Cheung, S. Y. et al. TRPC4/TRPC5 channels mediate adverse reaction to the cancer cell cytotoxic agent (−)-englerin A. *Oncotarget* **9**, 29634–29643 (2018).
73. Müller, M. et al. Ideal efficacy photoswitches for TRPC4/5 channels harness high potency for spatiotemporally-resolved control of TRPC function in live tissues. Preprint at *bioRxiv* https://doi.org/10.1101/2024.07.12.602451 (2024).
74. Müller, M. et al. Ideal-efficacy photoswitches chromocontrol TRPC4/5 channel functions in live tissues. *figshare* https://doi.org/10.6084/m9.figshare.26232254.v1 (2025).
75. Zholos, A. V., Melnyk, M. I. & Dryn, D. O. Molecular mechanisms of cholinergic neurotransmission in visceral smooth muscles with a focus on receptor-operated TRPC4 channel and impairment of gastrointestinal motility by general anaesthetics and anxiolytics. *Neuropharmacology* **242**, 109776 (2024).

[1]Faculty of Chemistry and Food Chemistry, Dresden University of Technology, Dresden, Germany. [2]Department of Pharmacy, Ludwig-Maximilians University of Munich, Munich, Germany. [3]Rudolf-Boehm-Institute of Pharmacology and Toxicology, Leipzig University, Leipzig, Germany. [4]Center for Integrative Physiology and Molecular Medicine, Saarland University, Saarbrücken, Germany. [5]Leeds Institute of Cardiovascular and Metabolic Medicine, LIGHT Laboratories, University of Leeds, Leeds, UK. [6]Astbury Centre for Structural Molecular Biology, University of Leeds, Leeds, UK. [7]Department of Structural Biochemistry, Max Planck Institute of Molecular Physiology, Dortmund, Germany. [8]School of Biomedical Sciences, University of Leeds, Leeds, UK. [9]These authors contributed equally: Markus Müller, Konstantin Niemeyer. [10]These authors jointly supervised this work: Michael Schaefer, Oliver Thorn-Seshold. ✉e-mail: michael.schaefer@medizin.uni-leipzig.de; oliver.thorn-seshold@tu-dresden.de

## Methods

Materials and methods including chemical synthesis, photophysical data and NMR spectra are available in the Supplementary Information.

## Acknowledgements

This research was supported by funds from the German Research Foundation (DFG: SFB TRR 152 number 239283807 projects P24 to O.T.-S., P18 to M.S., P02 to S.R., P10 to F.Z. and T.L.-Z., P07 to Y.S. and D.B.; SFB 1032 project B09 number 201269156, SPP 1926 project number 426018126 and Emmy Noether grant 400324123 to O.T.-S.; SFB 894 number 157660137 project A17 to F.Z. and T.L.-Z.), the Biotechnology and Biological Sciences Research Council (BBSRC; BB/P020208/1 to R.S.B.), the British Heart Foundation (PG/19/2/34084 to C.C.B.) and the Max Planck Society (to S.R.). Large-scale tissue culture at the University of Leeds was performed in the Asbury Protein Production Facility, funded by the University of Leeds and the Royal Society (WL150028). Cryo-EM work at Leeds was performed at the Astbury Biostructure Laboratory, funded by the University of Leeds and Wellcome Trust (108466/Z/15/Z, 221524/Z/20/Z and 218785/Z/19/Z). M. Müller thanks the Joachim Herz Foundation for fellowship support. A.V.J. thanks the BBSRC for a White Rose DTP PhD studentship. E. Gouaux (Vollum Institute) is kindly acknowledged for providing the BacMam vector. M. Freichel (Heidelberg) is kindly acknowledged for providing the TRPC4/5-KO mice. O.T.-S. thanks R. Leurs, M. Decker, P. Gorostiza, W. Szymanski and J. Frank for feedback on the prior reports of efficacy switches.

## Author contributions

As related to Figs. 1a–j and 2h–j, M. Müller designed the targets and performed the synthesis and photochemical evaluation, as supervised by O.T.-S. M. Müller and O.T.-S. performed the mechanistic analysis and modeling. As related to Figs. 1k–n, 2a–g and 6, K.N., N.U. and F.B. performed all experiments as designed and supervised by N.U. and M.S. M.S. analyzed the data and drafted the corresponding paper sections and figures. As related to Fig. 3a–d, S.A.P. performed the protein expression and purification, cryo-EM data collection, processing and model building and data analysis. C.C.B. designed and cloned the TRPC4 and TRPC5 plasmids. A.V.J. performed the intracellular calcium recordings and analyzed the data. S.A.P. and A.V.J. made the figures. S.P.M and R.S.B designed and supervised the experiments and obtained funding. R.S.B. wrote sections of the paper with input from S.A.P., C.C.B, A.V.J. and S.P.M. As related to Fig. 3e–h, D.V. performed the protein expression and purification, as well as cryo-EM data collection and processing, under the supervision of S.R. As related to Fig. 4, K.O. and M. Makke performed all the experiments related to chromaffin cells and hippocampal neurons, which were designed, supervised and analyzed by Y.S. and D.B., who drafted the corresponding paper sections and figures. As related to Fig. 5, N.K.O., F.Z. and T.L.Z. designed, performed, analyzed and drafted the paper for all experiments related to the mouse hypothalamus. M.S. and O.T.-S. designed the study. M. Müller and O.T.-S. performed overall data and figure assembly and wrote the paper with input from all authors.

## Competing interests

R.S.B. is a cofounder and partner of the pharmaceutical start-up company CalTIC. R.S.B. and S.A.P. have received funding from CalTIC. The other authors declare no competing interests.

## Additional information

**Supplementary information** The online version contains supplementary material available at https://doi.org/10.1038/s41589-025-02085-x.

**Correspondence and requests for materials** should be addressed to Michael Schaefer or Oliver Thorn-Seshold.

**Peer review information** *Nature Chemical Biology* thanks Wiktor Szymanski, Weiping Wang and the other, anonymous reviewer(s) for their contribution to the peer review of this work.

nature portfolio

Corresponding author(s): Oliver Thorn-Seshold, Michael Schaefer

Last updated by author(s): Oct 14, 2025

# Reporting Summary

Nature Portfolio wishes to improve the reproducibility of the work that we publish. This form provides structure for consistency and transparency in reporting. For further information on Nature Portfolio policies, see our Editorial Policies and the Editorial Policy Checklist.

## Statistics

For all statistical analyses, confirm that the following items are present in the figure legend, table legend, main text, or Methods section.

| n/a | Confirmed |
|---|---|
| ☐ | ☒ The exact sample size (*n*) for each experimental group/condition, given as a discrete number and unit of measurement |
| ☐ | ☒ A statement on whether measurements were taken from distinct samples or whether the same sample was measured repeatedly |
| ☐ | ☒ The statistical test(s) used AND whether they are one- or two-sided<br>*Only common tests should be described solely by name; describe more complex techniques in the Methods section.* |
| ☒ | ☐ A description of all covariates tested |
| ☐ | ☒ A description of any assumptions or corrections, such as tests of normality and adjustment for multiple comparisons |
| ☐ | ☒ A full description of the statistical parameters including central tendency (e.g. means) or other basic estimates (e.g. regression coefficient) AND variation (e.g. standard deviation) or associated estimates of uncertainty (e.g. confidence intervals) |
| ☐ | ☒ For null hypothesis testing, the test statistic (e.g. *F*, *t*, *r*) with confidence intervals, effect sizes, degrees of freedom and *P* value noted<br>*Give P values as exact values whenever suitable.* |
| ☒ | ☐ For Bayesian analysis, information on the choice of priors and Markov chain Monte Carlo settings |
| ☒ | ☐ For hierarchical and complex designs, identification of the appropriate level for tests and full reporting of outcomes |
| ☒ | ☐ Estimates of effect sizes (e.g. Cohen's *d*, Pearson's *r*), indicating how they were calculated |

*Our web collection on statistics for biologists contains articles on many of the points above.*

## Software and code

Policy information about availability of computer code

| | |
|---|---|
| Data collection | As related to Figure 1: Figure 1k-n (and S2, S12 and S13): Fluo-4 fluorescence signals were recorded in a custom-made Fluorescence Imaging Plate 182 Reader (FLIPR) built into a robotic liquid handling station (Freedom Evo 150, Tecan, 183 Männedorf, Switzerland) using a Zyla sCMOS camera (Andor, 189 Belfast, UK) and the controlling software Micromanager (Edelstein et al., 2010). Figure 1c-d, S9-11: Absorption was measured with a Agilent Cary60 Spectrophotometer, irradiation carried out with a CoolLED pE-4000 and controlling software Micro-Manager.<br>As related to Figure 2: Electrophysiological experiments were performed at room temperature using a Multiclamp 700B amplifier with a Digidata 1440A digitizer (Axon CNS, Molecular Devices, Sunnyvale, CA) controlled with PClamp 10 software (Molecular Devices). Figure 2 h-j, Table S3: PSS data was collected on a HPLC (details see supporting information).<br>As related to Figure 3: TRPC5 structural biology: Cryo-EM data were collected using the standard EPU data collection software installed by FEI EPU 3.1. TRPC4 structural biology: Cryo-EM datasets were collected using the commercially available software EPU version 2.8<br>As related to Figure 4:Electrophysiological recordings were peformed using HEKA Pulse 8.2 software (Lambrecht, Germany); Image of TRPC5 IC R26 tGFP positive neuron was taken with VisiView software (Visitron, Germany).<br>As related to Figure 5: Data acquisition upright scanning confocal microscope (Zeiss LSM 880 Indimo) equipped with a standard Argon laser for GCAMP6f excitation at a wavelength of 488 nm and a UV laser (Coherent) emitting 355 nm for photoswitching; Zen<br>As related to Figure 6: Figure 6b,c, Figure S23b, and Video S5: Optical recordings of intestinal motility were obtained with a Zyla sCMOS camera (Andor, Belfast, UK) and the controlling software Micromanager (Edelstein et al., 2010). Figure 6e-h and Figure S23c-g: Contractile forces were measured and digitized with a 4-channel multi myograph system (DMT 620M, Danish Myo Technology, Hinnerup, Denmark), controlled with aLabChart Pro V8 software.<br>As related to Figure S8: Intracellular calcium measurements used the SoftMax Pro 7 software. |
| Data analysis | As related to Figure 1k-n (S2a-d, S12 and S13): Micromanager/Fiji; c-d, S9-11: GraphPad Prism 10 |

| | |
|---|---|
| Data analysis | As related to Figure 2: Clampfit 10.7, h-j: GraphPad Prism 10 and Agilent ChemStation<br>As related to Figure 3: TRPC5 structural biology: Data was pre-process (Motion correction and CTF estimation) in CryoSPARC v4.1 while particle picking, and data processing was done in Cryosparc v4.4. Initial model was generated using ModelAngelo, and manually adjusted in Coot (0.9.8.8) while for model refinement we used PHENIX (1.20.1). Model validation, as reported in the paper was conducted using PHENIX and Molprobity. UCSF ChimeraX (1.6) was used for visualisation and figure preparation. TRPC4 structural biology: Data collection was monitored live using TranSPHIRE. Intial motion correction and dose weighting was done with MotionCor2 v.1.3.0 and CTF estimation with CTFFIND 4.1.131. SPHIRE software package version 1.4 was used for Particle extraction and 2D classification. Particles were picked automatically with crYOLO version 1.8. 3D classification and refinement was performed with Relion v 3.1 and CryoSPARC v 4.0. Protein model building was carried out in coot v 1.9 and further refined by Phenix v 1.18.2. Figures were prepared in Chimera v 1.15 and Chimera X v 1.7.1. Pore analysis has been done by Pore Walker online Software.<br>As related to Figure 4: Data was analysed using IgorPro 5.0 and SigmaPlot 13.<br>As related to Figure 5: ImageJ, Igor Pro (Wavematrics), OriginLab v. 2020.<br>As related to Figure 6: Figure 6b,c: MicroManager 2.0 gamma and MS Excel. Figure 6e-h: LabChart Pro V8 (ADInstruments) and MS Excel<br>As related to Figure S8: Analysis of data from intracellular calcium measurements was performed using GraphPad Prism 8, 9, 10 |

For manuscripts utilizing custom algorithms or software that are central to the research but not yet described in published literature, software must be made available to editors and reviewers. We strongly encourage code deposition in a community repository (e.g. GitHub). See the Nature Portfolio guidelines for submitting code & software for further information.

## Data

Policy information about availability of data

All manuscripts must include a data availability statement. This statement should provide the following information, where applicable:

- Accession codes, unique identifiers, or web links for publicly available datasets
- A description of any restrictions on data availability
- For clinical datasets or third party data, please ensure that the statement adheres to our policy

All data needed to evaluate the conclusions in the paper are present in the paper. Data are deposited in BioRxiv (https://doi.org/10.1101/2024.07.12.602451), or on Figshare (Fig. 5, https://doi.org/10.6084/m9.figshare.26232254.v1), or on PDB and EMDB as related to Figure 3 (TRPC4:E-AzPico, 3.0 Å, PDB 9FXL (https://doi.org/10.2210/pdb9FXL/pdb), EMDB 50850; TRPC4:Z-AzPico, 3.1 Å, PDB 9FXM (https://doi.org/10.2210/pdb9FXM/pdb), EMDB 50851; hTRPC5:E-AzHC, 2.6 Å, PDB 9G4Y (https://doi.org/10.2210/pdb9G4Y/pdb), EMDB 51074; hTRPC5:Z-AzHC, 2.9 Å, PDB 9G50 (https://doi.org/10.2210/pdb9G50/pdb), EMDB 51076).

## Research involving human participants, their data, or biological material

Policy information about studies with human participants or human data. See also policy information about sex, gender (identity/presentation), and sexual orientation and race, ethnicity and racism.

| | |
|---|---|
| Reporting on sex and gender | n/a |
| Reporting on race, ethnicity, or other socially relevant groupings | n/a |
| Population characteristics | n/a |
| Recruitment | n/a |
| Ethics oversight | n/a |

Note that full information on the approval of the study protocol must also be provided in the manuscript.

# Field-specific reporting

Please select the one below that is the best fit for your research. If you are not sure, read the appropriate sections before making your selection.

☒ Life sciences ☐ Behavioural & social sciences ☐ Ecological, evolutionary & environmental sciences

For a reference copy of the document with all sections, see nature.com/documents/nr-reporting-summary-flat.pdf

# Life sciences study design

All studies must disclose on these points even when the disclosure is negative.

| | |
|---|---|
| Sample size | As related to Figure 1k-n (S2, S12, S13): A cell suspension was used and all experiments were conducted as a minimum of 3 independent experiments with each experiment averaging data in technical duplicates.<br>As related to Figure 2d-g: Data as means and S.E. were obtained from 12 different cells, in our hand a sufficient number to estimate electrophysiological activity of a compound when using a clonal HEK293 cell line.<br>As related to Figure 3: Structural biology of TRPC4: For AzPico E isomer, 2,598 movies were collected. 214,819 particles were picked and for final reconstruction and 139,750 particles were used; For AzPico Z isomer 3,311 movies were collected. 232983 particles were picked and for final reconstruction and 93651 particles were used.<br>As related to Figure 4: This experimental design for electrophysiological recordings is based on years of research experience conducting these |

types of experiments (e.g. Schwarz et al., 2019; Kollewe et al., 2022). Statistical analysis was conducted on the collected data, taking into account the number of cells in each experiment. No specific statistical tools were used to predetermine the sample size. The sample sizes were chosen to provide sufficient statistical power to detect biologically significant differences between experimental treatments. All key experiments supporting the main conclusions of the study were repeated several times in samples prepared from at least 3 animals obtained from different litters.
As related to Figure 5: Sample sizes are estimated based on previous physiological studies using similar animal models to guarantee statistical relevance. The number of animals used is a minimum necessary to provide adequate data to test the hypotheses of this project. We have minimized the number of animals required by the animal welfare committees wherever possible. PHYSIOLOGY: Tissue from a single animal remains maximally viable for a full day's experiments. However, due to animal viability, cell viability, and experimental variables it is impossible to predict how many responding cells can be successfully recorded in a given day's work. The significance of a particular recording, and hence the judgment as to whether it must be repeated, can only be made after the recordings are analyzed. Some experiments required tissue from 3-5 different animals. Any less data would fail to meet statistical significance.
As related to Figure 6: As related to Figure 6b and Figure S23b: optical recordings of intestinal motility were obtained from 10 intestinal segments obtained from a single C57Bl6/N mouse.

As related to Figure 6e-h and Figure S23c-g: Data are representative traces obtained from 2-4 intestinal segments per animal. Segments from four 7- to 10-week-old male (TRPC5-/-) and five (TRPC4-/-) mice were investigated for each genotype and genetic background (TRPC4-/- mice, matching wild-type mice, TRPC5-/- mice, and their matching wild-type.
As related to Figure S8: intracellular calcium recordings were used to show that the point mutants generated led to TRPC channels that retained sensitivity to (-)-englerin A but did not necessarily retain sensitivity to AM237 / Z-AzHC. Sample size calculations were not considered applicable to these studies. The number of repeats was deemed sufficient to support the conclusions drawn.

Data exclusions

As related to Figure 1: There was no data excluded.
As related to Figure 2d-g: Using a clonal HEK293 cell line stably expressing YFP-tagged mTRPC4ß enabled the selection of mTRPC4-positive cells by fluorescence signal and avoided a strong mean variation. Only 1 measurement of 12 cells was excluded from statistical analysis because maximal activity was too small to obtain a realistic action spectra.
As related to Figure 3: TRPC5 structural biology: No data were excluded. TRPC4: During cryo-EM dataset processing, false picks during particle picking were eliminated and further particles that does not contribute to high resolution features has been removed based on 2D and 3D classification which is a standard procedure.
As related to Figure 4: There was no data excluded.
As related to Figure 5: Recordings were excluded in the determination of the dose-response curves, when a cell was not responding to any stimulation. Otherwise no data were excluded.
As related to Figure 6: There was no data excluded.
As related to Figure S8: At most, one outlier well per plate was excluded e.g. in the case that transfection had not succeeded in that well. Independent replicates are not shown.

Replication

As related to Figure 1k-n (S2, S12, S13): Reproducibility was was ascertained by performing measurements on 3 several days, with technical duplicates.
As related to Figure 2d-g: Reproducibility of electrophysiological results was ascertained by performing measurements on several days.
As related to Figure 3: TRPC5 structural biology:N/A; no clinical samples or animal samples were used. Randomization is used CryoSPARC to estimate the final resolution of cryo-EM maps. TRPC4: All cryo-EM datasets were acquired once as it is unattainable to repeat the cryo-EM dataset collection and processing of the same sample from the time and cost perspective.
As related to Figure 4: All experiments were performed from at least three independent preparations and measurements.
As related to Figure 5: Multiple measurements using different mice in each experimental and control groups were performed to check reproducibility of results. As has been our practice throughout the manuscript, we use at least three animals per experiment.
As related to Figure 6: 10-12 repeated photoswitching cycles were applied in parallel measurements of 2-4 intestinal segments. Experiments were repeated at three different days, using segments obtained from different animals
As related to Figure S8: Total repeats (N) are shown in Figure S4. Independent replicates are not shown.

Randomization

As related to Figure 3: During final cryo-EM dataset reconstruction particles were randomly split into two equal subsets for FSC calculation.
As related to Figure 4: Wildtype and corresponding knock out cells were prepared and measured on the same day in a random fashion.
As related to Figure 5: To eliminate the potential influence of batches of physiological solutions or solutions of photoswitchable compounds, the experiments with wild-type and knockout Trpc5 animals were conducted on the same day. Furthermore, changes in the concentration of photoswitchable compounds were randomized to exclude adaptive responses or mistakes in washing out a particular concentration from the external solution.

Blinding

Investigators were not blinded for this study (not relevant to cellular or ex vivo studies with automated objective readout by machines)

# Reporting for specific materials, systems and methods

We require information from authors about some types of materials, experimental systems and methods used in many studies. Here, indicate whether each material, system or method listed is relevant to your study. If you are not sure if a list item applies to your research, read the appropriate section before selecting a response.

## Materials & experimental systems

| n/a | Involved in the study |
|---|---|
| ☐ | ☒ Antibodies |
| ☐ | ☒ Eukaryotic cell lines |
| ☒ | ☐ Palaeontology and archaeology |
| ☐ | ☒ Animals and other organisms |
| ☒ | ☐ Clinical data |
| ☒ | ☐ Dual use research of concern |
| ☒ | ☐ Plants |

## Methods

| n/a | Involved in the study |
|---|---|
| ☒ | ☐ ChIP-seq |
| ☒ | ☐ Flow cytometry |
| ☒ | ☐ MRI-based neuroimaging |

# Antibodies

Antibodies used

rabbit anti-Th (1:1000, polyclonal, #ab112, Abcam; RRID:AB_297840) ; donkey anti-rabbit-Alexa555 (1:1000, #A31572, Thermo Fisher; RRID:AB_162543); unconjugated AffiniPure Fab fragment goat anti-mouse IgG (H+L; #115-007-003, Jackson ImmunoResearch; RRID:AB_2338476); mouse anti-Trpc5 (1:500, monoclonal; clone N67/15, NeuroMab, Davis, CA; RRID:AB_2240979); biotinylated goat anti-mouse IgG2b antibody (1:400, #115-065-207, Jackson Immuno Research; RRID:AB_2338573); Alexa 488-conjugated streptavidin (1:200; S-32354, Invitrogen; RRID:AB_2315383)

Validation

For negative controls, antibody dilution buffer without primary antibodies was applied. The exact same batch of mouse anti-Trpc5 (1:500, monoclonal; clone N67/15, NeuroMab, Davis, CA; RRID:AB_2240979) antibody was investigated in TRPC5-deficient mice (Blum et al., 2019, Proceedings of the National Academy of Science USA).

# Eukaryotic cell lines

Policy information about cell lines and Sex and Gender in Research

Cell line source(s)

As related to Figures 1-2: Human embryonic kidney (HEK293) cell line (ATCC CRL-1573); stably transfected with cDNA of mouse TRPC4ß-YFP or TRPC5-YFP.
As related to Figure 3: TRPC5 structural biology: Freestyle 293F (ThermoFisher Scientific, R79007).
As related to Figure S8: HEK293 (ATCC CRL-1573).

Authentication

We did not authenticate the HEK293 cell lines.

Mycoplasma contamination

We did not test for mycoplasma contamination.

Commonly misidentified lines
(See ICLAC register)

No commonly misidentified cell lines were used in this study.

# Animals and other research organisms

Policy information about studies involving animals; ARRIVE guidelines recommended for reporting animal research, and Sex and Gender in Research

Laboratory animals

As related to Figure 4: TRPC1/C4/C5 triple knock out, TRPC5 single knock out mice and TRPC5 IC eR26 tGFP were generated as described previously (Bröker-Lai et a., 2017; Schwarz et al., 2019; Kollewe et al., 2022). Trpc1/4/5−/− and TRPC50/- mice were compared to C57BL/6N mice, which were obtained from Charles River and housed under the same conditions as the knockout (KO) animals. For hippocampal neuron preparations, animals of either sex were prepared postnatal day 0. Mouse chromaffin cells were prepared from adult male mice (10-12 weeks old)
As related to Figure 5: We used following mouse strains: 1. Th-GCaMP6f mice (produced by crossing mouse strain 'Th-Cre mice', also called B6.Cg-7630403G23RikTg(Th-cre)1Tmd/J (RRID:IMSR_JAX:008601 with mouse strain R26-GCaMP6f, also called B6;129S-Gt(ROSA)26Sortm95.1(CAG-GCaMP6f)Hze/J (RRID:IMSR_JAX:024105, ror Ai95D mice). 2. Th-GCaMP6f-ΔTrpc5 (produced by crossing Th-GCaMP6f mice with Trpc5-E5−/− mice (Trpc5tm1.1Lbi (RRID:IMSR_JAX:024535; MMRRC Stock No: 37349-JAX). All mice were Adult female mice (7 - 20 weeks old).
As related to Figure 6: mus musculus, C57Bl6/N strain (CharlesRiver) wild-type or homozygous TRPC4-/- and homozygous TRPC5-/-, backcrossed to the C57Bl6/N strain (CharlesRiver) for at least seven generations. Mice were housed in groups of two to three animals under approved standard conditions of a 12 h light-dark-regime and access to food and water ad libitum. Strains for testing intestinal contractility were C57BL6/N mice (from Charles River) and homozygous TRPC5 or TRPC4 single knockout mice(Freichel et al. Nat. Cell Biol. (2001) 3:121-127 PMID: 11175743), both back-crossed on the C57BL6/N background for at least five generations. All mice were of male sex. For myography experiments, intestinal segments were prepared from mice at the age of 4-7 months. Wild-type control mice were matched in age to the respective knock-out animals.

Wild animals

The study did not involve wild animals.

Reporting on sex

As related to Figure 4: For hippocampal neuron preparations, animals of either sex were prepared postnatal day 0. Only adult male mice were taken for chromaffin cell preparations. To avoid hormonal differences in adult mice influencing the response, we specifically chose only male mice.
As related to Figure 5: From the study of Blum et al. (2019) PNAS, it is evident that only female mice having a Trpc5 deficiency result

| | |
|---|---|
| | in hypoprolactinemia and altered function of oscillatory TH+ neurons in the arcuate nucleus. This is the rationale behind the decision to utilize only female mice in the experiments of Figure 5 and S22.<br>As related to Figure 6: In myography experiments, a total of 18 male mice (9 wild-type, 5 TRPC4-/- and 4 TRPC5-/- mice) have been investigated. Since expression of TRPC4 in the intestine is not reported to differ between male and female mice, we do not expect relevant differences between sexes. |
| Field-collected samples | The study did not involve samples collected from the field. |
| Ethics oversight | As related to Figure 4: All mice were kept according European Animal Welfare regulations and ethical guidelines from the local governing body (Nr Az. 2.4.1.3/ Bruns).<br>As related to Figure 5: Animal care and experimental procedures were performed in accordance with the guidelines established by the German Animal Welfare Act, European Communities Council Directive 2010/63/EU, the institutional ethical and animal welfare guidelines of the Saarland University (approval number of the Institutional Animal Care and Use Committee: CIPMM-2.2.4.1.1).<br>As related to figure 6: The study does not involve animal experiments. All tissues were explanted from animals that were previously sacrificed by decapitation. |

Note that full information on the approval of the study protocol must also be provided in the manuscript.

## Plants

| | |
|---|---|
| Seed stocks | n/a |
| Novel plant genotypes | n/a |
| Authentication | n/a |